# Eco-evolutionary dynamics of temperature niche evolution during range expansions

**A Thesis**

submitted to
Indian Institute of Science Education and Research Pune
in partial fulfillment of the requirements for the
BS-MS Dual Degree Programme

by

Saismit H Naik


Indian Institute of Science Education and Research Pune
Dr. Homi Bhabha Road,
Pashan, Pune 411008, INDIA.

December, 2022

Supervisor: Dr Emanuel Fronhofer

# Certificate

This is to certify that this dissertation entitled Eco-evolutionary dynamics of temperature niche evolution during range expansionstowards the partial fulfilment of the BS-MS dual degree programme at the Indian Institute of Science Education and Research, Pune represents study/work carried out by Saismit H Naikat Indian Institute of Science Education and Research under the supervision of Dr Emanuel Fronhofer, CNRS Researcher, Department of Biology , during the academic year 2022-2023.

Saismit Naik
20171142
BSMS-IISER Pune

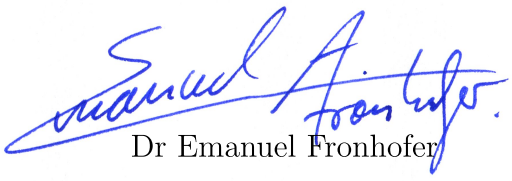

Dr Emanuel Fronhofer

Committee:

Dr Emanuel Fronhofer

Dr Sutirth Dey

This thesis is dedicated to my laptop.

# Declaration

I hereby declare that the matter embodied in the report entitled Eco-evolutionary dynamics of temperature niche evolution during range expansions are the results of the work carried out by me at the Department of Biology, Indian Institute of Science Education and Research, Pune, under the supervision of Dr Emanuel Fronhofer and the same has not been submitted elsewhere for any other degree.

Saismit Naik
20171142
BSMS-IISER Pune

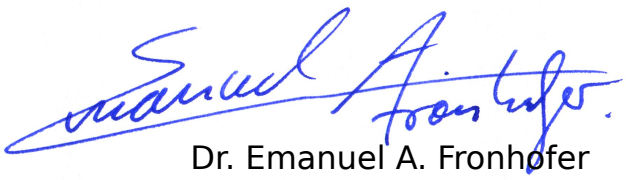

Dr. Emanuel A. Fronhofer

# Acknowledgments

Firstly, I would like to thank my supervisor Dr.Emanuel Fronhofer for the brilliant guidance and constant encouragement I received throughout the thesis. I would also like to thank Jhelam, Vandana, Sasha, the EEC team at ISEM, Satavisha and Koustav for their company without which I couldn't have managed living abroad for the first time. I thank Dr.Sutirth Dey for his insightful comments during the Mid-year assessment which helped shape the course of my project. I am also grateful to Dr.Suhita Nadkarni for her invaluable mentorship in my fledgling years that helped me stand on my own feet. Finally I thank my family for being unconditionally supportive of my decisions during the last five years.

# Abstract

Climate change is predicted to change the distribution of species worldwide. Predictive models are required to help forecast these ecosystem responses. However, to build such models, the mechanisms behind the ecological and evolutionary dynamics of species distributions need to be better understood. One central driver and modulator of eco-evolutionary dynamics is temperature and its changes due to human impacts, for example. Yet, temperature dependence of ecological and evolutionary processes is often modelled in very simplified ways with unrealistic assumptions. To build a more productive theory of the temperature impacts in ecology and evolution, I take a bottom-up approach, integrating molecular mechanisms and large-scale population dynamics: I study how different assumptions of protein level dynamics that constrain thermal evolution may scale up to the macroecological level and change range dynamic predictions. Importantly, this mechanistic approach allows me to include likely targets of selection and model feedback with the evolutionary dynamics of local adaptation of the thermal performance curve (TPC) and dispersal. I build an individual-based metapopulation model of range expansion along a temperature gradient. Using three different models of thermal adaptation at the protein level, I show the importance of the mechanism considered under selection in determining range expansion trends. The TPCs described by protein thermal stability are more flexible and lead to accelerated expansion along an increasing temperature gradient. While TPCs described by enzyme-substrate reaction rates are much less flexible and lead to much slower expansion. Overall, my project shows the importance of defining TPCs realistically and its large-scale consequences.

# Contents

# List of Figures

# List of Tables

# Introduction

Understanding and forecasting the dynamics of species distributions is a central challenge in ecology and evolution. Traditionally, species' ranges have been considered from a purely ecological perspective driven by their abiotic environment. However, recent evidence suggests that both rapid evolution and biotic factors may play important roles [85, 75] that have led to more nuanced insights regarding biodiversity under global change [74]. To improve our understanding of forces driving the shift under climate change and the eco-evolutionary feedback that would be generated, it is important to understand how dispersal processes and local adaptation of species to novel temperatures would interact [4].

Dispersal ability is a heritable trait and subject to evolution [86, 46] driving regional dynamics. The rapid evolution of dispersal ability and local adaptation in expanding species ranges has been empirically observed [54, 22, 19]. When *Drosophila subobscura* was introduced to North America, it evolved the clinal variation in wing size, spanning more than 15 degrees of latitude as observed in Europe [54]. Wing size reduced from cold to hot, with a noticeable change emerging within 2 decades. The hypothesised mechanism is increasing wing area compensated for reduced wing beat frequency in colder temperatures [42]. Similar latitudinal clines are observed with life history traits in *Lythrum salicaria*, a highly invasive plant in North America. Earlier flowering was observed in colder regions with shorter growing seasons resulting in smaller plants while in the hotter regions late flowering but bigger-sized plants were selected for [22]. A more recent study on damselflies *Ischnura elegans* who have seen to be rapidly expanding their ranges polewards didn't show evolution across temperatures of a faster life history but due to lowered metabolic rate and increased feeding rate, larvae evolved faster development rate at the hotter rearing temperature. Further theoretical studies expect the evolution of dispersal ability to interact with environmental gradients to affect invasion speed and available genetic variation at the range fronts [53]. With projected

climate change, many species are expected to shift their ranges in response to rising habitat temperatures [49].

Temperature is an important determinant of biological rates across scales of hierarchy, but there is still a lack of understanding of the underlying mechanisms of thermal evolution. Local adaptation to new temperatures is determined by the thermal performance curves (TPCs) of organisms, i.e., an individual's fitness as a function of temperature. Physiological, ecological and interactive biological rates often show a steep initial rise with lower temperatures. Hence, the Metabolic theory of ecology (MTE) drew analogy to rising temperatures increasing collision between molecules and suggested that the Boltzmann–Arrhenius model from chemical reaction kinetics can be used to fit the rise of many biological rates with temperature [15, 29, 44]. For enzyme-catalysed reactions, temperature increases the likelihood of enzyme-substrate collisions, which increases reaction rates. But excessive increase can break intramolecular bonds in proteins and lead to denaturation, decreasing reaction rates. The underlying assumption is that species do not experience extreme temperatures to lie in the decreasing part of the TPC. Hence thermal performance curves have been predominantly described by an exponential function despite evidence of a unimodal curve on a wide enough temperature range [29, 93, 111, 31, 5]. But with predicted climate change, many species are set to experience inhospitable temperatures [102].

Temperature dependence of enzyme kinetics translates to similar dependence of metabolic rate and individual growth rates on temperature. The effect is felt strongly by ectotherms where increased metabolic reactions may decrease energy allocation to growth and reproduction. Further interspecific variations in temperature sensitivity of population and individual growth rate affect community dynamics and assembly [61]. Analysis by Dell et al. [29] on a wide range of TPCs for traits covering several levels of organisation found that TPCs were widely unimodal, left-skewed curves. The Boltzmann-Arrhenius equation showed a good fit with the rising phase of the curve with a small range for the activation energies observed. The range of activation energies or the exponential scaling factors observed were within the range observed for metabolic reactions. But the scaling consequences of temperature makes it daunting to understand the mechanisms underlying effect of temperature on population dynamics. Recent progress has been made at understanding effect of temperature at the level of single proteins [36, 52] but not of their eco-evolutionary implications. Theoretical evolutionary studies of TPCs to understand thermal evolution have relied on quantitative genetics models owing to the complex genetic architecture underlying it [16].

Abstract asymmetric TPCs are often assumed with no mechanistic basis. But model results are strongly dependent on assumed trade-offs such as generalist-specialist trade-offs, which have not found much evidence in experiments, but the 'hotter is better' trade-offs based on thermodynamic effects has found better support [16]. Hence I wish to understand the thermodynamic implications of changing temperature on growth rates from first principles.

Taking into account the unimodality of TPCs is of central importance for prediction-making. Studies that have considered the empirical unimodal and skewed TPC concluded that the inclusion of asymmetry in fitness curves in ecological models suggests asymmetric responses of species along latitudes, such as in response to climate fluctuations [103, 70]. The asymmetry is predicted to strengthen selection at warm than at cold temperatures. A study in the fly *Sepsis punctum* from northern, central and southern Europe was measured for divergence in juvenile development rate at 5 experimental temperatures. They found that hot development temperatures were associated with lower genetic variances for all cases [10, 27]. At a community level, theory predicts that consumer-resource interactions where the maturation rate of resources are more temperature sensitive i.e with narrower breadth of their TPC than their consumers, are more susceptible to extinction from warming. Resource maturation rate decreases with the temperature at the fall of their developmental rate TPC, and higher mortality at very low and very high temperatures of adult resource population limits the consumers' thermal range. If the consumer is less sensitive to temperature change, then they end of exploiting the resource at a faster rate with increase in temperature [3].

Adaptive evolution studies have found biochemical or biophysical properties of metabolically important proteins show latitudinal clines [13]. Recent work by [7] put forward a general theory of temperature dependence of biological rates using the Eyring equation, a mechanistic analogue of the Boltzmann-Arrhenius equation, which is widely accepted as the basis for temperature scaling of chemical reaction rates. It is derived from the Macromolecular Rate Theory [51] that suggests that biological rates are modulated by temperature as it changes the rigidity and stability of the activated enzyme-substrate complex during biomolecular reactions. They argue that the inclusion of the effect of temperature on the entropy of activation of the transition state complex is enough to explain the wide variety of TPCs observed as the equation provides a good fit over many organisational levels and taxa. But it is difficult to comment on the mechanism behind thermal evolution from the goodness of fit. Genetics of protein evolutions are highly constrained by epistasis, which result in a rugged genotype-phenotype map [13, 47]. Mechanisms other than the increased effect of

temperature on the entropy of activation of enzyme-substrate complex may be limiting population growth at high temperatures. It is difficult to formulate a single integrating theory, especially when there can be various protein level changes for the same stress [110, 83].

My project investigates the effect of different mechanisms underlying thermal evolution at lower-level processes of protein reaction rates whose unimodal dependence is better studied and how it may affect higher-level population growth responses. First, I performed a literature review to identify mechanistic models of temperature scaling at the microscopic level. Subsequently, I incorporated these protein-level mechanistic models into a general population growth model taking differential impacts of birth, death and density dependence into account. This allows me to derive TPCs with different underlying assumptions regarding the mechanisms responsible for temperature scaling. In addition, I assessed empirical support for the evolutionary potential of different model parameters which ultimately allows me to include TPC evolution into my model. Second, I used the model system *Tetrahymena thermophila*, a freshwater ciliate, to confront these models with empirical growth rate data. Bayesian fitting allows me to identify more and less supported TPC models. Finally, I use simulations to investigate the macroscopic consequences of assuming different TPCs models for range expansion dynamics. For this final part of my work, I have developed a continuous-time individual-based range expansion model that includes an abiotic temperature gradient. Importantly, the model is eco-evolutionary in that both TPCs and dispersal, as well as interaction strengths, are subject to evolution.

# Chapter 1

# Literature review

Several models have attempted to understand the rise and fall of enzyme kinetics in response to temperature more mechanistically [30, 51, 20, 56, 82, 90, 39]. Overall there seem to be two major mechanisms being proposed which are either temperature dependence of protein folding or of enzymatic rates. For a given series of chemical reactions, there is a series of enthalpy ($\Delta H_i$), entropy ($\Delta S_i$), and free energy ($\Delta G_i$) changes, which are individually related as follows:

$$\Delta G_i = \Delta H_i - T\Delta S_i \tag{1.1}$$

Based on the statistical mechanical justification of the transition state theory, the Eyring-Polanyi equation describes how the rate of chemical kinetics should change with temperature. The rate constants ($k_i$) are related as follows:

$$k_i = \frac{k_B T}{h} e^{\Delta \frac{S_i}{R}} e^{\Delta \frac{-H_i}{RT}} \tag{1.2}$$

where $k_B$ is the Boltzmann constant, $h$ is Planck's constant, $\Delta H_i$ is the enthalpy of activation that is the enthalpy difference between transition complex and the active form, $\Delta S_i$ is the entropy of activation. Enthalpy change is the heat absorbed during the reaction or in case of protein-ligand reactions sum of the bond energies of the bonds broken during a reaction minus the sum of the bond energies of the bonds formed during the reaction. Entropy change relates to the number of ways energy can be distributed in a system. Entropy is higher where there are more ways to distribute energy. Proteins that can adopt many different conformations have more ways to distribute energy and are higher in entropy than proteins

whose movements are constrained. Bonds within proteins are all associated with specific amounts of energy; when more movements are possible, there are more ways to distribute energy.

When $\Delta H_i$ and $\Delta S_i$ are considered constant, the Eyring equation is analogous to the empirical Arrhenius equation. But temperature affects conformational stability of proteins changing fraction of proteins in their native state and binding affinities of enzymes. Further $\Delta H_i$ and $\Delta S_i$ of protein folding and protein-ligand reactions are temperature dependent. The theory used to describe the same considers a temperature-independent heat capacity to describe the nonlinear temperature dependence of free energy $\Delta G$ and is given by:

$$T\frac{\Delta S_i}{dT} = \Delta C_p \tag{1.3}$$

$$\frac{\Delta H_i}{dT} = \Delta C_p \tag{1.4}$$

Therefore temperature dependence of $\Delta H_i$ and $\Delta S_i$ for a reference temperature $T_0$:

$$\Delta H_T^{\ddagger} = \Delta H_{T_0}^{\ddagger} + \Delta C_p(T - T_0) \tag{1.5}$$

$$\Delta S_T^{\ddagger} = \Delta S_{T_0}^{\ddagger} + \Delta C_p \ln\left(\frac{T}{T_0}\right) \tag{1.6}$$

A major assumption when these equations have been used to describe higher-level properties such as metabolism and growth rate is that, on average the higher-level property follows the same functional form as a single protein-level reaction. Mathematical models have found a good fit for such assumptions for large data sets [23, 64]. It is also possible that the steps involved have similar temperature dependence as found in yeast glycolytic enzymes [25] though there hasn't been a consensus [92].

Multiple studies on metabolically crucial enzymes have shown evolution to temperature with ligand binding and catalytic rate being under selection [36, 13]. These properties can be changed by both evolution of flexibility and stability of proteins and enzymes. But pervasive epistasis can severely restrict the trajectories that protein evolution can take [47]. Proteins with similar folds and functions can have different sequences, and mutations will affect them differently. But when sequentially similar proteins are subject to selection for the same stress, they have a shared set of mutational trajectories as they have similar constraints and epistatic interactions [76, 47].

For example, Couñago et al. [24] replacing the gene for adenylate kinase, an important metabolic enzyme in a thermophile, makes it poorly adapted to its environment. After 1500 generations, sequencing showed mutations that increased the stability and activity of the enzyme at higher temperatures and the new structure of the protein being slightly different from its wild type. Clonal bacterial strains grown at across a range of temperatures showed different pathways of cold and hot evolution at their growth temperature with different trade-offs though some were more common than others [9]. The effect of evolutionary history may be strong and strongly constrain thermal evolution. Hence amino acid substitutions in one species environment may not be beneficial in another species' environment [14, 99, 110, 107]. A single mechanism of thermostability may not arise to deal with the same thermal stress [48]. Hyperthermophiles share the same catalytic mechanisms as their mesophilic counterparts. Analysis of the molecular mechanism behind the thermostability of hyperthermophilic and thermophilic enzymes suggests use of multiple mechanisms to increase thermodynamic stability, including increasing stability across the temperature range, shifting the stability curve to higher temperatures, or flattening the stability curve or a combination of them though increasing melting temperature. [105, 83]

To summarise, when considering the effect of thermal evolution through changes in protein level properties, it is important to consider that there can be multiple means to the same end. Overall, protein thermal stability could change, [105, 83] or there can be changes to enzyme properties which influence rates of biochemical reactions [73] or both. Changes in enzyme thermal stabilities may also affect their catalysis efficiency [36]. Hence, I wish to consider modelling three major mechanisms that have been considered to be controlling the thermal evolution of reactions rates:

- Temperature dependence of protein denaturation

- Temperature dependence of enzyme reaction rates

- Temperature dependence enzyme denaturation on enzyme reaction rates

## 1.1 Proteome Model

Johnson and Lewin[56] noticed that *Escherichia Coli* grown at 45 °C ceased to grow but started to grow exponentially when shifted to 37 °C. They declared that cells underwent reversible damage. They assumed one master enzyme ($E_n$) limits the population growth rate:

$$s(T) = E_n \frac{k_B T}{h} e^{\frac{-\Delta_{G_i^\ddagger}}{RT}} \tag{1.7}$$

The enzyme can go from a native form to a denatured form reversibly:

$$\mathrm{E}_n \underset{\mathrm{k_2}}{\overset{\mathrm{k_1}}{\rightleftharpoons}} \mathrm{E}_d \tag{1.8}$$

In its native state, a protein has low enthalpy and conformational entropy, while both increase when it denatures. The effective energy of a protein is the intra-protein interactions and the protein solvent interactions that change as it folds and unfolds. A protein unfolds when the energy of its native state becomes equal to its unfolded state, i.e. $\Delta G$ between folded and unfolded equals zero. Point mutations seem to mostly affect the energy (or enthalpy as the difference is negligible at normal pressures) of the native state of the proteins [113]. Equilibrium concentrations are given as:

$$\frac{k_1}{k_2} = \frac{E_n}{E_d} = e^{\frac{-\Delta_G}{RT}} \tag{1.9}$$

Where $\Delta H$ is the enthalpy difference and $\Delta S$ is the entropy difference between active and inactive forms. If $E_0$ is the total amount of enzyme:

$$E_n = \frac{E_0}{1 + e^{\frac{-\Delta_G}{RT}}} \tag{1.10}$$

Substituting Eqn. 1.10 in Eqn. 1.7 completes the model:

$$s(T) = \frac{E_0 k_B T e^{\frac{-\Delta_{G_i^\ddagger}}{RT}}}{h(1 + e^{\frac{-\Delta_G}{RT}})} \tag{1.11}$$

Chen and Shakhnovich [20] use the above model and link the replication rate of an organism to the functionality of each protein encoded by the essential genes. This assumption

was motivated by recent experiments that showed the knockout of a few 'essential' genes is enough to confer a lethal phenotype [38]. Therefore an organism is assumed to be viable if all its essential genes encode stable proteins. Further, greater protein stability is not assumed to confer greater fitness i.e. it is a neutral trait. The frequency of each rate-determining protein $i$ (RDP) with $\Delta G_i$ is given by:

$$f_i = \frac{1}{1 + e^{\frac{-\Delta_{G_i}}{RT}}} \tag{1.12}$$

Therefore temperature scaling $s(T)$ is given by :

$$s(\Delta G, T) = b_0 \frac{e^{\frac{-\Delta_{H^\ddagger}}{RT}}}{\prod_{i=1}^{n} 1 + e^{\frac{-\Delta_{G_i}}{RT}}} \tag{1.13}$$

where n is the number of RDPs, $\Delta H^\ddagger$ is the metabolic free energy barrier. Temperature dependence of $\Delta G_i$ is given by (combining Eqn. 1.20 and Eqn. 1.21):

$$\Delta G_i(T) = \Delta H_r + \Delta C_p(T - T_r) - T\Delta S_r - \Delta C_p T \ln\left(\frac{T}{T_r}\right) \tag{1.14}$$

where $T_r, \Delta H_r, \Delta S_r$ are the reference temperature, enthalpy change at $T_r$, entropy change at $T_r$ respectively. $\Delta C_p$ is assumed to be constant. It is further modified:

$$\Delta G_i(T) = \Delta G_i(T_r) + \Delta C_p(\delta T) - \delta T\Delta S_r + \Delta C_p T_r \ln\left(\frac{T_r + \delta T}{T_r}\right) \tag{1.15}$$

where $\delta T = T - T_r$. As $\frac{\delta T}{T_r} << 1$ and reduce the expression to a linear dependance:

$$\Delta G(T) = \Delta G(T_r) - \delta T\Delta S_r \tag{1.16}$$

I consider the model by Chen and Shakhnovich [20] for a single RDP:

$$s(\Delta G(T_r), \Delta S_r) = b_0 \frac{e^{\frac{-\Delta_{H^\ddagger}}{RT}}}{1 + e^{\frac{-\Delta_{G(T)}}{RT}}} \tag{1.17}$$

### 1.1.1 Empirical support

The key premise of the model proposed by Chen and Shakhnovich [20] is that thermal evolution of individual growth rate occurs by modulating copy numbers of folded proteins given by Eqn. 1.12. It results in a 'Hotter is better' trend as seen in Fig. 3.2- I J as protein denaturation occurs at higher temperatures and the exponential rise at lower temperatures does not change with changes in the activation free energy and entropy for denaturation at lower temperatures. Support for such a trend has been found with viruses, bacteria and insects [16, 39, 60]. Studies with *Escherichia Coli* adapted at a higher temperature have been shown to out-compete bacteria reared at the original environmental temperatures [26, 63] suggesting a lack of evolutionary trade-off with growth at lower temperatures for evolution to hotter temperatures. Further, a recent analysis [98] found evidence of stability compensation in the metabolically important enzyme Ketosteroid isomerase (KSI) in hot versus cold variants of the bacteria *Pseudomonas putida* and found a lack of rate compensation. Though cellular proteomes are known to have a wide distribution of thermal stability, and a recent study in *Escherichia Coli* checked if loss of cell viability at high temperatures occurs due to global protein denaturation but found that few thermal-sensitive proteins were under stronger selection, [13] implying a drop in the copy number of these folded proteins will reduce growth rate. The study, Chen and Shakhnovich [20], fitted their equation data used by Ratkowsky et al. [81] consisting of 35 sets of data for thermal evolution of different bacteria strains, with 2 free parameters, $\Delta H^{\ddagger}$ and $n$, number of RDPs, and found a good fit. Hence the proposed model is applicable in cases where thermal evolution primarily occurs by changing in folded fractions of a small number of essential proteins. The model does not explicitly consider the number of folded proteins and only considers the fraction of folded proteins. It does not consider an increase in growth rate by increase in protein copies though a smaller number of copies may select for faster evolution of new phenotypes, as recently shown by [58].

### 1.1.2 Evolving variables

In the above model, after using a first-order approximation, the parameters describing the scaling function are the activation free energy for denaturation, $\Delta G(T_r)$, and the activation entropy of denaturation, $\Delta S_r$ at the reference temperature $T_r$. Evolutionary potential for both these paramters has been observed. As noted by Zeldovich et al. [113] most point

mutations in proteins seem to be changing the activation-free energy and as noted before increase in thermal stability of proteins has been observed in certain taxa as means of evolution to hotter temperatures [98, 13]. Entropy-changing mutations in *Escherichia coli*'s adenylate kinase are important for cold adaptation [88]. Such flexibility increasing changes in protein sequences have been widely identified in psychrophilic enzymes [94, 35].

## 1.2 Macromolecular rate theory model

Recently, Hobbs et al. [51] put forth the Macromolecular rate theory, an alternative model to describe the unimodality of enzyme rate kinetics based on the transition state theory [32]. It considers temperature dependence of the Gibbs energy of activation for protein ligand interactions as I described before Eqn. 1.20 and Eqn. 1.21.

$$\Delta G_i^{\ddagger} = \Delta H_i^{\ddagger} - T\Delta S_i^{\ddagger} \tag{1.18}$$

$$k_i = \frac{k_B T}{h} e^{\Delta \frac{S_i^{\ddagger}}{R}} e^{\Delta \frac{-H_i^{\ddagger}}{RT}} \tag{1.19}$$

Therefore temperature scaling $s(T)$ is given by for a reference temperature $T_r$:

$$\Delta H_T^{\ddagger} = \Delta H_{T_r}^{\ddagger} + \Delta C_p (T - T_r) \tag{1.20}$$

$$\Delta S_T^{\ddagger} = \Delta S_{T_r}^{\ddagger} + \Delta C_p \ln\left(\frac{T}{T_r}\right) \tag{1.21}$$

$$s(\Delta H_{T_r}^{\ddagger}, \Delta S_{T_r}^{\ddagger}, \Delta C_p) = \frac{k_B T}{h} e^{\frac{\Delta_{S_T^{\ddagger}}}{R}} e^{\frac{-\Delta_{H_T^{\ddagger}}}{RT}} \tag{1.22}$$

### 1.2.1 Empirical support

The Macromolecular rate theory [51], in contrast to our previous model, assumes that the fall in the TPC curve occurs due to the temperature dependence of the enthalpy and entropy change accompanying enzyme-substrate reactions. The temperature dependence is linear and scaled by the heat capacity. Explanation of the curvature of the TPC by protein denaturation is inadequate as enzymes have been observed to lose their activity at lower temperatures than their denaturation temperatures especially in psychrophilic enzymes [34]. For negative heat

capacity changes during enzyme-substrate reactions, the increase in rate at temperatures is driven by the enthalpic term in Eqn. 1.20 but with increasing temperatures, term is taken over by the entropic term Eqn. 1.21. To shift $T_{opt}$ higher or lower , $\Delta C_p$ values need to increase and decrease respectively. This correlation has been demonstrated by Hobbs et al. [51] by mutagenesis on enzyme barnase and studying reaction kinetics data from IPMDH enzymes of mesophilic and psychrophilic *Bacillus* species. Increasingly negative $\Delta C_p$ can be achieved by increasing the $C_p$ of enzyme substrate complex and/or decreasing the $C_p$ of the enzyme transition-state species. It would result in a higher $K_M$ and $k_{cat}$ for the enzyme, leading to stronger enzyme-substrate binding which has been observed to show thermal evolution in both interspecific and intraspecific comparisons [52, 92, 96, 13]. Further, the model has been used to characterise soil microbial growth rates [2] and leaf respiration [65]. To summarise, the Macromolecular rate theory may be applicable when enzymes lose their activity before they denature as is often seen in cold adapted enzymes. The $\Delta C_p$ values are expected to increase for lower optimal temperatures while for hotter optimal temperatures they will increasingly tend towards 0.

### 1.2.2 Evolving variables

As discussed above, changes in heat capacity change may be important for thermal evolution especially at colder temperatures. Large variation of heat capacity is seen among enzymes [2, 114]. Further, a study on modern hyperthermophilic, mesophilic, and psychrophilic organisms change in transition state heat capacity as the evolution driver of fitness in different temperature niches [73]. Heat capacity term serves to describe the temperature dependence of enthalpy and entropy changes to explain the curvature of the TPC.

But since I consider evolution of the TPC is also important to look at the evolutionary potential of the enthalpy ($\Delta H^{\ddagger}_{T_r}$) and entropy changes ($\Delta S_{T_r}$) accompanying enzyme substrate reactions. Changes in enthalpy and entropy of enzyme-substrate bonding are related through the phenomena of Enthalpy-Entropy Compensation (EEC) [84, 66, 37]. Stronger covalent binding results in a large negative enthalpy change but reduces mobility resulting a large negative entropic change. Similarly, positive entropy increase may result in positive enthalpic change as interactions are disrupted. For example, in psychrophilic enzymes, the dampening of catalytic activity by lowered temperature is increased by a lower activation enthalpy in order to increase their turnover. This is structurally achieved by a decreasing

energy releases during bond breaking and forming during protein denaturation and folding, i.e enthalpic changes, leading to a more flexible structure [67, 35]. For enzyme-subtrate reactions, which are modeled by the Macromolecular Rate Theory [51], it would mean that a high flexibility comes with a reduced binding affinity in the enzyme substrate complex [51, 37]. The relationship of enthalpy and entropy change or between activation energy and pre-exponential factor during protein denaturation and folding has been measured [84, 79, 12] and has often found to be approximately linear. Similar assumption was made by Grimaud [45] for fitting the Hinshelwood model [50] to TPCs of phytoplankton. I will try to incorporate the trend by constraining the model to have a linear relationship between the terms $\Delta H^{\ddagger}_{T_r}$) and $\Delta S_{T_r}$.

## 1.3 Enzyme-Assisted Arrhenius Rate model

Till now the models above have assumed a maximum growth rate that reduces with increasing temperature as enzymes lose their catalytic ability. But enzymes reduce the free energy barriers of biological reactions and increase the reaction rate from a baseline. DeLong et al. [30] propose the Enzyme-Assisted Arrhenius Rate (EAAR) model taking into consideration the thermostability of enzymes on reduced free energy barrier for the reaction. Mechanistic derivations of protein stability curves give that the temperature dependence of $\Delta G$ follows from combining Eqn. 1.20 and Eqn. 1.21 with a further simplification for protein folding by considering $T_m = T_0$, where $T_m$ is the melting temperature at which $\Delta G_i = 0$ and represents the midpoint for transition from native to denatured state [33]:

$$\Delta G = \Delta H \left(1 - \frac{T}{T_m}\right) + \Delta C_p \left(T - T_m - T \ln \frac{T}{T_m}\right) \tag{1.23}$$

The EAAR model suggests that the enzyme lowers the activation energy $E_b$ by $E_{\Delta H}$ for change in enthlapy and $E_{\Delta C_p}$ with respect to change in heat capacity, The total decrease in activation energy ($E_c$) is given by:

$$E_c = E_{\Delta H} \left(1 - \frac{T}{T_m}\right) + E_{\Delta C_p} \left(T - T_m - T \ln \frac{T}{T_m}\right) \tag{1.24}$$

$$s(E_H, E_{C_p}, T_m) = b_0 e^{\frac{E_b - E_c}{kT}} \tag{1.25}$$

### 1.3.1 Empirical support

The EAAR model uses the protein thermostability to describe how increase in unfolded enzymes increases activation energy as temperatures rise. Though its parameters have mechanistic meaning it obscures whether they describe an averaged phenomena or dependency of a single enzyme. The model has been applied to *Paramecium bursari* population growth rate curves and predicts increased enthalpy of reaction and greater enzyme heat capacity, which can be achieved by changing enzyme thermal stability or introduction of heatshock proteins [69]. Fitting the model on TPC of population growth rates of zebra mussels found that thermal evolution seems to occur through changing the melting temperature ($T_m$) parameter. It could suggest the increase in thermal stability of the membrane-embedded protein oxidative phosphorylation complexes that has been shown to be an important rate limiting factor in aerobic metabolism [30]. Since the EAAR model assumes a functional relationship between fraction of enzymes in folded state and the reduction in the activation energy, it is more abstract than the other two models and can be used to get insight into mechanisms underlying thermal evolution in different environments.

### 1.3.2 Evolving variables

The EAAR model is considering the same mechanism as Proteome model, that is the thermostability of enzymes except it is considering the effect of enzyme denaturation on the enzyme reaction rate. The model is assumes a linearly relationship between unfolded enzymes and decrease in metabolic activation energy by them. As noted by the authors it is difficult to assign a particular mechanism behind each of the free paramters $E_{\Delta C_p}$, $E_{\Delta H}$ and $E_{\Delta T_m}$ but changes in each affects the TPC differently and hence it provides multiple pathways for the TPC to evolve along.

# Chapter 2

# Methods

## 2.1 Thermal Performance Curve fitting

I fit the three models to observed temperature population growth data of freshwater ciliate *Tetrahymena thermophila* of mating type I. These microorganisms are increasingly used as model organisms in ecology and evolution [40]. Data has been collected from a strain kept at $20°C$ and assayed for population growth at at ten different temperatures: $25, 10, 15, 20, 25, 30, 33, 36, 39, 40°C$ over 3 weeks with 5 replicates. I used posterior distributions of population growth rates extracted from the empirical times series by fitting a modified continuous time logistic growth model, with decay in carrying capacity after a threshold time, to the population density estimates using Bayesian statistical model from *rstan* R packages [97].

Using this already existing data set of fitness (population growth rate) as a function of temperature, I fitted the three TPC models: Proteome model (Eqn. 1.7), MMRT model (Eqn. 1.22) and EAAR model (Eqn. 1.23), to the estimated population growth rates using Bayesians statistical tools in R version 4.2.1 'rstan' [97] and 'brms' [18] which allowed for the propagation of the error associated with growth rate posterior distributions. I used 4 Markov chain Monte Carlo (MCMC) chains of 10,000 iterations for each replicate and model and visually checked for convergence. Maximum tree depth was 15 and adapt delta was 0.999. Uninformed Gaussian priors were used with approximate means of expected magnitude. R code used for fitting can be found in the Supplementary Material.

I performed model selection on the fits, using three information criterions: Akaike Information Criterion (WAIC) [106], Pareto Smoother Importance Sampling - Leave One Out Pseudo Bayesian Model Averaging (PSIS-LOO) [104] and Bayesian stacked weights of PSIS-LOO [112]. I use more than one information criterion as pWAIC is found to be high when computing WAIC, hence I use the PSIS-LOO averaging. I also use Bayesian stacked weights which is good for similar models and it keeps weight of the best model unchanged.

## 2.2 Individual-Based Model

In order to explore the macroscopic consequences of assuming different temperature scaling models of underlying mechanisms as described above, I use a stochastic, individual-based model to simulate the population dynamics of a single species in a landscape with $n$ identical patches using a Gillespie algorithm [43]. My model is based on a continuous-time version of the discrete Beverton-Holt population growth model with emigration [11].

$$\frac{dN_x}{dt} = \frac{b}{(1+\beta N_x)}N_x - dN_x - eN_x + \frac{e(1-\mu)N_{x+1}}{2} + \frac{e(1-\mu)N_{x-1}}{2} \tag{2.1}$$

where $N_x$, $N_1$ and $N_n$ are populations of the species in the $x^{th}$, $1^{st}$ and last patch respectively. $b$ is the species birth rate, $d$ is the death rate, $e$ is the emigration rate, $\mu$ is the emigration mortality and $\beta$ is the intraspecific competition coefficient

Individuals in the model are asexual and can move to the neighboring patch. They are characterized by traits describing the temperature scaling functions for birth rate ($b$) associated with the three models: Proteome model (Eqn. 1.7), MMRT model (Eqn. 1.22) and EAAR model (Eqn. 1.23); temperature scaling of death rate (($d$) and emigration rate ($e$). Emigration mortality ($\mu$) are kept constant for all individuals ($N$).

In each time step an individual may experience one of the three events: birth, death or emigration. To choose the event, I follow the modified Gillespie algorithm by Allen and Dytham, 2009 [1]. To understand the modification, in a direct Gillespie algorithm:

1. Probabilities of giving birth, death or dispersing for an individual $i$ are given by its trait $b_i, d_i, e_i$, respectively.

2. Each time-step is picked from an exponential distribution with mean $\lambda = \Sigma(b_i+d_i+e_i)$.

3. The next event is calculated where The probability of birth, death or dispersal for individual $j$ is $\frac{b_j}{\Sigma(b_i+d_i+e_i)}$, $\frac{d_j}{\Sigma(b_i+d_i+e_i)}$ and $\frac{d_j}{\Sigma(b_i+d_i+e_i)}$ respectively.

Each event requires rates to be calculated for every member of the population. In the modified Gillespie algorithm, per event calculation is independent of population size, which implies and important gain in simulation time:

1. Probabilities of giving birth, death or dispersing for an individual $i$ are given by its trait $b_i, d_i, e_i$, respectively.

2. Each time-step is picked from an exponential distribution with mean $\lambda = (c_b+c_d+c_e)N$ where $c_b >= max(b_i : \forall i)$, $c_e >= max(e_i : \forall i)$ and $c_d >= max(d_i : \forall i)$.

3. The event is selected where The probability of birth, death or dispersal is $\frac{c_b}{(c_b+c_e+c_d)}$, $\frac{c_e}{(c_b+c_e+c_d)}$ and $\frac{c_d}{(c_b+c_e+c_d)}$ respectively.

4. For individual $j$ the The probability of the selected event occurring is $\frac{b_j}{c_b}$, $\frac{e_j}{c_e}$ and $\frac{d_j}{c_d}$ respectively.

5. The next event is selected where the The probability of birth, death or dispersal for individual $j$ is $\frac{c_b}{(c_b+c_e+c_d)}$, $\frac{c_e}{(c_b+c_e+c_d)}$ and $\frac{c_d}{(c_b+c_e+c_d)}$, respectively.

The birth rates, death rates, and intraspecific competition coefficient were assumed to scale with temperature. Details of temperature scaling are given below.

### 2.2.1 Birth

The continuous-time Beverton-Holt model can be derived mechanistically assuming that a focal population of individuals consumes an abiotic resource (following a chemostat model) with a linear, Lotka-Volterra-type, functional response [101]. Using a time-scale separation argument one can obtain the dynamics of the focal consumer population as follows:

$$\frac{dN}{dt} = \frac{caS}{1+\frac{a}{w}N}N - dN \tag{2.2}$$

where $w$ is the flow rate of resources in and out of the system, $S$ is the constant resource flowing into the system, $c$ is the efficiency of resource consumption, $a$ is the feeding rate. Considering $b = eaS$ and $\beta = \frac{a}{w}$:

$$\frac{dN}{dt} = \frac{b}{1 + \beta N} N - dN \tag{2.3}$$

In order to include temperature dependence into this model, note that both $b$ and $\beta$ are constant multiples of $a$ which has been shown to be temperature-dependent [28]. Hence, I assume that $\beta$ scales with the same exponential rate as $b$. Temperature scaling $s(T)$ defined by each of the three models: Proteome model (Eqn. 1.7), MMRT model (Eqn. 1.22) and EAAR model (Eqn. 1.23). Birth rate temperature dependence is given by:

$$\frac{dN}{dt} = \frac{b}{1 + \beta N} N - dN \tag{2.4}$$

Both $b$ and $\beta$ are constant multiples of $a$ which has been shown to be temperature-dependent [28], hence I assume that $\beta$ scales with the same exponential rate as $b$. Temperature scaling $s(T)$ defined by each of the three models. Birth rate temperature dependence is given by:

$$b_i(T) = b_0 s(T) \tag{2.5}$$

$b_0$ is calculated using approximately the observed birth rate of *Tetrahymena thermophila* [41] at 20°C :

$$b_0 = 0.15 s^{-1}(293K) \tag{2.6}$$

The temperature dependence of the intraspecific competition coefficient is assumed to scale at the same exponential rate as the birth rate:

$$\beta_i(T) = \beta_0 s(T) \tag{2.7}$$

where $\beta_0$ is:

$$\beta_0 = 0.004 s^{-1}(293K) \tag{2.8}$$

An event is selected by relative maximum rate constants. Hence, the The probability of birth event is :

$$\frac{c_b}{(c_b + c_d + c_e)} \tag{2.9}$$

taking density-regulation into account, the The probability of the birth event being executed is given by:

$$\frac{b_i}{(1+\beta_i N)c_b} \tag{2.10}$$

### 2.2.2 Emigration

Emigration is density-independent. The The probability of choosing an emigration event is given by:

$$\frac{c_e}{(c_b+c_d+c_e)} \tag{2.11}$$

The The probability of executing an emigration event is given by:

$$\frac{e_i}{c_e} \tag{2.12}$$

A dispersal cost is applied as emigration mortality $\mu$ if executed.

### 2.2.3 Death

Death rate temperature dependence is taken to be of the Boltzmann-Arrhenius equation form as has been widely observed [71] :

$$d(T) = d_0 e^{-(E)_i/RT} \tag{2.13}$$

where $d_0$ is calculated using the observed death rate of *Tetrahymena thermophila* [41] at 20 °C:

$$d_0 = 0.05 e^{(E)_i/293R} \tag{2.14}$$

All individuals have equal death rates. The probability of choosing a death event is given by:

$$\frac{c_d}{(c_b+c_d+c_e)} \tag{2.15}$$

The probability of executing a death event is given by:

$$\frac{d_i}{c_d} \tag{2.16}$$

### 2.2.4 Full birth-death model

Hence, the temperature-dependent logistic equation can be given as:

$$\frac{dN_x}{dt} = \frac{b_0 s(T)}{1 + \beta_0 s(T) N_x} N_x - d_0 e^{-E/RT} N_x \tag{2.17}$$

As temperature modulates the growth and death rate it also affects the number of individuals each patch can hold. Equilibrium density for the continuous-time Beverton-Holt model is given by:

$$\hat{N} = \frac{b - d}{d\beta} \tag{2.18}$$

Considering temperature dependence of the parameters:

$$\hat{N}(T) = \frac{b - d}{d\beta} = \frac{b_0 s(T) - d_0 e^{-E/RT}}{d_0 e^{-E/RT} \beta_0 s(T)} = \frac{b_0}{\beta_0 d_0 e^{-E/RT}} - \frac{1}{\beta_0 s(T)} \tag{2.19}$$

The above equation is an approximation as I am not considering dispersal here.

### 2.2.5 Initialisation and analysis

To see the effect of thermal evolution on the range expansion, the evolving parameters are the individual emigration trait and the individual temperature scaling function traits. I wish to compare range dynamcis with and without local adaptation as well as with and without dispersal evolution. I also wish to provide a control for the effect of asymmetry in the TPC. Hence I compare the mechanistic TPCs with a Gaussian TPC with mean $T_0$ and standard deviation $\sigma$. The temperature scaling function is given by:

$$s(T) = b_0 e^{\frac{(T - T_0)^2}{2(\sigma)^2}} \tag{2.20}$$

The individual traits are given by the mean $T_0$ and standard deviation $\sigma$.

To keep relevant controls, for each model: Proteome model (Eqn. 1.7), MMRT model (Eqn. 1.22), EAAR model (Eqn. 1.23) and the Gaussian Curve (Eqn. 2.20), four simulations are run and are summarised in Fig. 2.2:

1. With thermal adaption where free parameters specified in the previous section are allowed to evolve , with dispersal evolution

2. With thermal evolution, without dispersal evolution

3. Without thermal evolution, with dispersal evolution

4. Without thermal evolution, without dispersal evolution

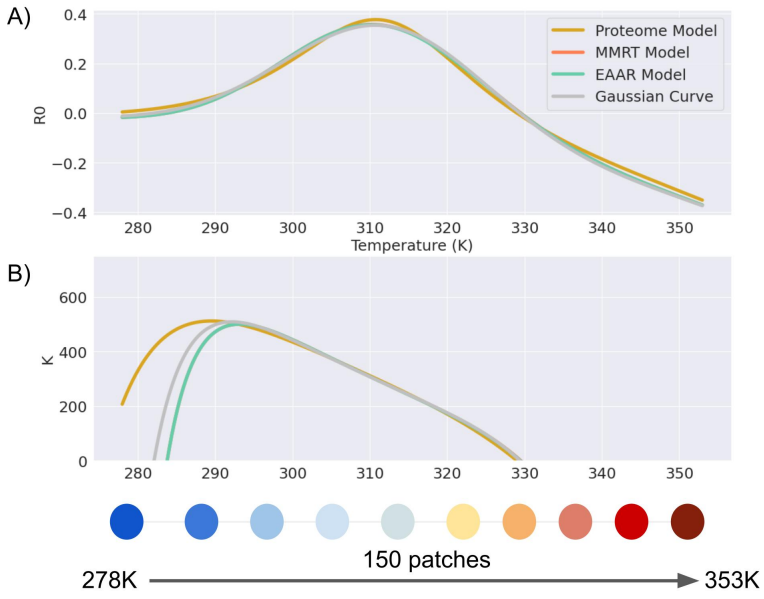


Figure 2.1: The linear landscape has 150 patches. Patch temperatures start from 278K and increase with a 0.5K step, till 353K. A) Growth rate given by Eqn. 2.6 for each model across the landscape. B) Carrying capacities across landscape, neglecting effect of dispersal and edge effects.

To minimise differences in initialisation, Proteome model, MMRT model and a Gaussian curve were fitted to a fixed EAAR curve using a least square algorithm to derive the initial parameters for each. The resulting curves can be seen in Fig. 2.1.

The metapopulation model consists of a 150-patch linear landscape. Each patch is kept at a fixed temperature and temperature increases linearly from 278K to 353K as shown in Fig. 2.1. The central 10 patches, i.e., the patches with temperatures from 55K to 65K are initialised with 200 individuals each. Dispersal to either ends of the landscapes is not allowed for the first 2000 hours to let the individual traits evolve to an equilibrium in the central patches as can be seen in Fig. 5.11 . After 2000 hours of burn-in, which is nearly 9500

generations on average in the ecological control in a patch at 20 C, individuals can disperse across the whole landscape.

All TPC models were run for the four scenarios in Fig. 2.2. 40 replicates are run for each case and temperature scaling model described in the previous section: EAAR model Proteome model, MMRT model. I output the population density of each patch, mean and interquartile range of each mutating parameter, every 2 hours in simulation time. I stop the simulations when the first replicate reaches either end of the landscape.

I compare the range front speeds between the four models under consideration. As the population is initialised at the centre of the landscape, there are two range fronts, one along an increasing temperature gradient and another along a decreasing temperature gradient. I hereby refer to the first as the 'hot range front' and the second as the 'cold range front'. The ecology control is the MMRT model's ecology control for both the cases with and without dispersal evolution. As the patch front dynamics of the ecology controls for all models are similar, as seen in Fig. 5.9 and Fig. 5.10, I do not show them all.

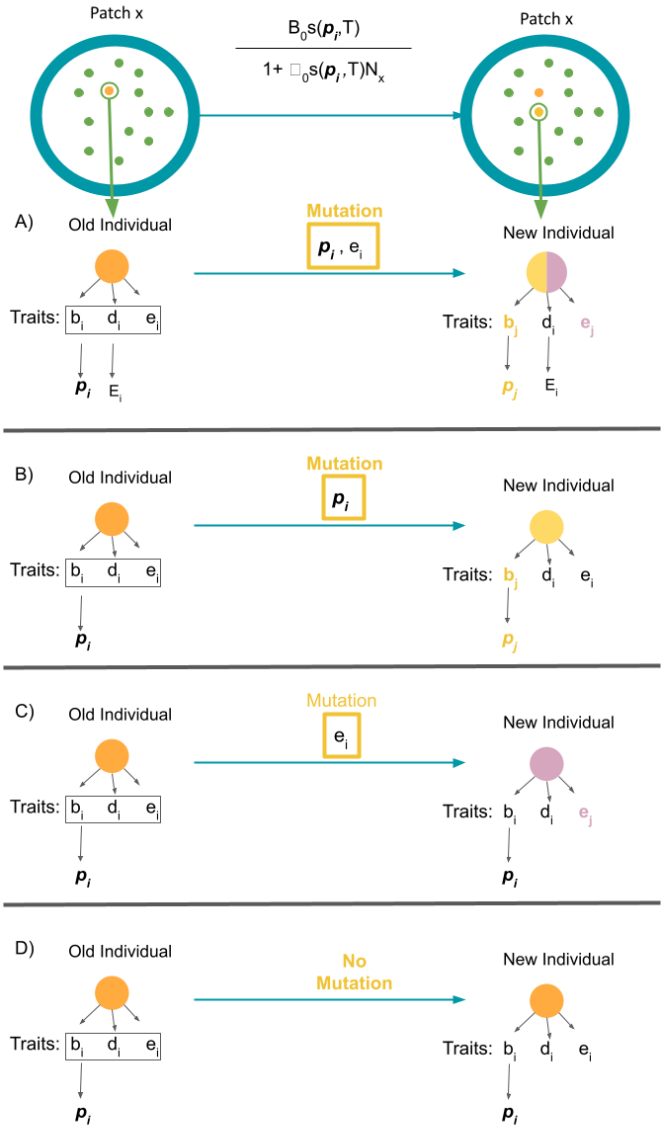


Figure 2.2: If a birth event chosen, individual $i$ reproduces with a probability proportional to the density-dependent birth rate where $N_x$ is total population in the patch $x$ as in Eqn. 2.10. Each thermal adaptation model is run with ecological controls for both the dispersal trait and the thermal adaptation traits. Hence the four cases are: A) Parameters describing the TPC $p_i$ and the emigration trait mutates at birth; B) Parameters describing the TPC $p_i$ and not the emigration trait mutates at birth; C) Parameters describing the TPC $p_i$ do not mutate and only the emigration trait mutates at birth; D) No trait mutates so the individual clones itself at birth. Hence with 3 alternative models of the TPC, I have 12 scenarios.

### 2.2.6 Evolution

In the simulations with evolution, the mutating parameters start with standing genetic variation given by a Gaussian curve whose standard deviation is the mean rounded down to the nearest variable of 10. At each birth, the traits may evolve with the probability 0.01. The evolved trait values are chosen from a Gaussian mutation kernel whose mean is the same as the mean of the parent individual and standard deviation is a magnitude less than the initial standard deviation. For each model, evolving parameters and their mutational kernels are given in the Tables 2.2, 2.3 and 2.5.

#### Model parameters and variables

Table 2.1: Common parameters for all simulations. Mean values are utilised for the dispersal traits when they are not mutating. Mutation kernel distribution is a Gaussian curve. The probability of mutation is 0.01.

| IBM Parameters | Description | Value |
|---|---|---|
| $N_x$ | Population density in patch $x$ | Initial value: 200 for patch 55-65 |
| $\beta$ | Intraspecific competition coefficient at 20 °C | 0.004 |
| $d$ | Death rate of all individuals at 20 °C | 0.05 |
| $b$ | Birth rate of all individuals at 20 °C | 0.15 |
| $e_i$ | Emigration rate of individual $i$ | 0.01, Initial: uniform distribution $[0, 0.2]$, Mutation S.D: a magnitude less than the nearest decimal |
| $\mu$ | Dispersal cost | 0.01 |
| $T$ | Temperature | 5-80 °C with 0.5 °C increase per patch |

Table 2.2: Parameters for the MMRT model of the TPC. All mutational kernels and initialisation are Gaussian curves. The standard deviation (SD) are given for both. The probability of mutation is 0.01 for each parameter.

| MMRT Model Parameters | Description | Value |
|---|---|---|
| $\Delta H^{\ddagger}_{T_0}$ | Enthalpy change at 20 °C | Mean: 0.05 eV, Initial S.D: 0.01, Mutation S.D: 0.001 |
| $\Delta S^{\ddagger}_{T_0}$ | Entropy change at 20 °C | Mean: -0.0015 eV, correlated $\frac{(\Delta_{H^{\ddagger}_{T_0}}-0.5)}{300}$ |
| $\Delta C_p$ | Heat capacity change | Mean: -0.05 eV, Initial S.D: 0.01, Mutation S.D: 0.001 |
| $E$ | Activation energy for $d$ | 0.3 eV, does not evolve |

Table 2.3: Parameters for the EAAR model of the TPC. All mutational kernels and initialisation are Gaussian curves. The standard deviation (SD) are given for both. The probability of mutation is 0.01 for each parameter.

| Proteome Model Parameters | Description | Value |
|---|---|---|
| $\Delta H^{\ddagger}$ | Metabolic free energy barrier | 0.75 eV |
| $\Delta G_r$ | Activation free energy at 20 °C | -0.0091 eV, Initial S.D: 0.1, Mutation S.D: 0.01 |
| $\Delta S_r$ | Activation entropy at 20 °C | -0.0051 eV, Initial S.D: 0.001, Mutation S.D: 0.0001 |
| $E$ | Activation energy for $d$ | 0.3 eV, does not evolve |

Table 2.4: Parameters for the Proteome model of the TPC. All mutational kernels and initialisation are Gaussian curves. The standard deviation (SD) are given for both. The probability of mutation is 0.01 for each parameter.

| EAAR Parameters | Description | Value |
|---|---|---|
| $E_b$ | Baseline activation energy | 0.1 eV |
| $E_{\Delta C_p}$ | Lowered activation energy wrt $\Delta C_p$ | 0.05 eV, Initial S.D: 0.01, Mutation S.D: 0.001 |
| $E_{\Delta H}$ | Lowered activation energy wrt $\Delta H$ | 0.05 eV, Initial S.D: 0.01, Mutation S.D: 0.001 |
| $T_m$ | Enzyme melting temperature | 310.5 K, Initial S.D: 10, Mutation S.D: 1 |
| $E$ | Activation energy for $d$ | 0.3 eV |

Table 2.5: Parameters for the Gaussian curve model of the TPC. All mutational kernels and initialisation are Gaussian curves. The standard deviation (SD) are given for both. The probability of mutation is 0.01 for each parameter.

| EAAR Parameters | Description | Value |
|---|---|---|
| $T_0$ | Mean of the gaussian curve | 312 K, Initial S.D: 10, Mutation S.D: 1 |
| $\sigma$ | Standard deviation of the gaussian curve | 13 K, Initial S.D: 1, Mutation S.D: 0.1 |

# Chapter 3

# Results

## 3.1 Data fitting

Over the 3 replicates I found that the Proteome model fits best for replicate A and replicate B according to all the information criterion weights. Similarly for replicate C, the EAAR model gives the best fit. Hence there is no consensus on the best model to describe the data.

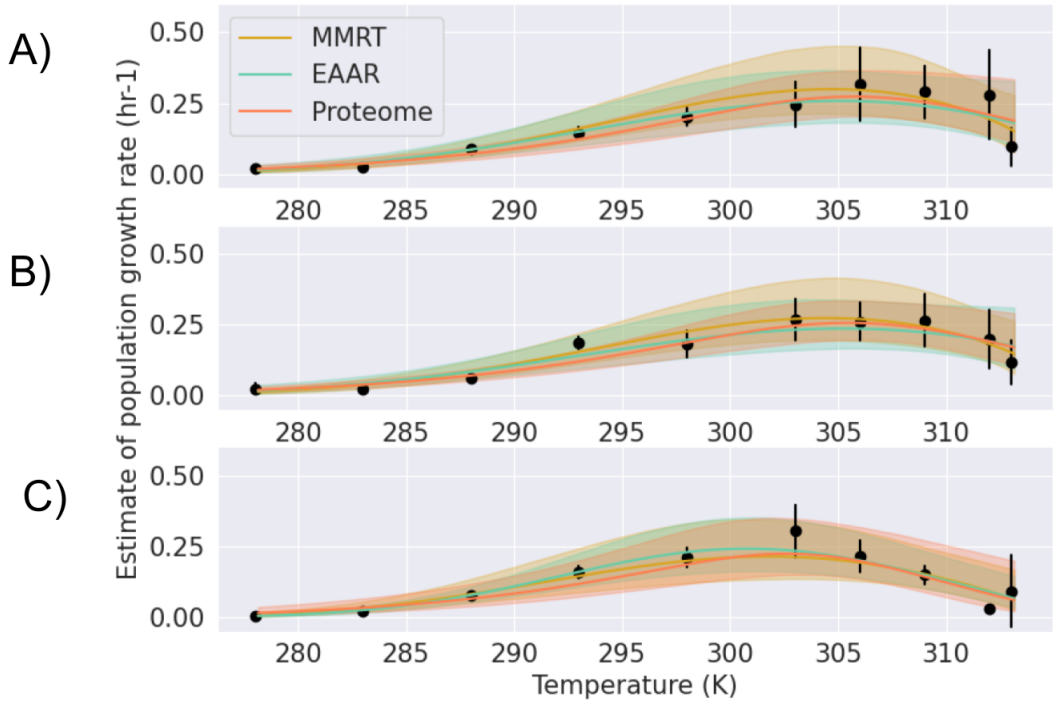


Figure 3.1: Fits of the three temperature scaling models to 3 replicates of TPC data for *Tetrahymena thermophila*. Black points represent experimental estimates of population growth rates, verical black lines show the 95% compatibility interval of the posteriors. The colored lines and corresponding shaded areas are posterior predictive means and 95% prediction intervals of the corresponding TPC models.

Table 3.1: Model selection for the 3 replicates. Column 1: Replicate and Models; Column 2: Weights for each model by the Akaike Information Criterion; Column 3: Weights for Pareto Smoother Importance Sampling - Leave One Out Pseudo Bayesian Model Averaging; Column 4: Bayesian stacking weights

| Replicate | WAIC | | | LOO | | | Stacking |
|---|---|---|---|---|---|---|---|
| A | IC | SE | Weight | IC | SE | Weight | |
| EAAR | 13.7 | 4.9 | 0.18 | 16.3 | 6.6 | 0.13 | 0 |
| Proteome | 11.7 | 5.7 | 0.48 | 13.5 | 7.0 | 0.55 | 0.65 |
| MMRT | 14.5 | 5.1 | 0.34 | 12.4 | 4.0 | 0.33 | 0.35 |
| B | | | | | | | |
| EAAR | 13.2 | 3.5 | 0.09 | 14.9 | 4.5 | 0.07 | 0 |
| Proteome | 8.7 | 3.6 | 0.82 | 9.8 | 4.9 | 0.087 | 1 |
| MMRT | 12.9 | 4.7 | 0.1 | 16.1 | 6.4 | 0.06 | 0 |
| C | | | | | | | |
| EAAR | 18.9 | 7.9 | 0.74 | 21.4 | 9.6 | 0.76 | 0.81 |
| Proteome | 24.7 | 5.2 | 0.04 | 26.3 | 6.0 | 0.06 | 0.19 |
| MMRT | 21.3 | 6.5 | 0.22 | 24.3 | 8.5 | 0.08 | 0 |

## 3.2 Modelling range expansion dynamics

### 3.2.1 Local adaptation without dispersal evolution

In the absence of dispersal evolution the Proteome model shows the fastest range expansion speeds on both the hot and cold fronts as seen in Fig. 3.3-B. The Proteome model follows a 'hotter is better' trend in thermal adaptation, i.e., adaptation to higher temperatures causes the maximum growth rate to rise. This hotter-is-better pattern is a consequence of modelling protein denaturation at higher temperatures. Hence, the exponential rise at lower temperatures does not change with changes in the activation free energy and entropy for denaturation, as seen in Fig. 3.2-I J. Increasing the activation free energy of denaturation increases stability and allows for exponential increase up to higher optimum temperatures, consequently increasing the maximum growth rate across the temperature spectrum. Therefore hotter adaptation also increases population growth rates at colder temperatures but not as much as for hotter temperatures. TPC at the end of the burn-in for both cold and hot fronts in Fig. 3.4-D are shifted rightwards and upwards, leading to a spatially increasing growth rate at the hot patch front in Fig. 3.3-C. Changes in activation free energy of denaturation seems to be the driving force behind thermal adaptation as the average value for the cold and hot patch fronts are much larger than the initialised values. There is not much difference for activation entropy. Further, there does not seem to be much difference between hot and cold patch front traits as in Fig. 5.1, confirming that an increase in activation-free energy is utilised for both cold and hot adaptation. As at the end of the burn in, the shifted TPC covers the whole hotter landscape there does not seem to be any directional change in the traits during range expansion accumulating lot more variation, which may be leading to the reduced growth rate of the equilibrium TPCs in Fig. 3.4-D.

Thermal evolution in the MMRT and EAAR model is much more constrained which is reflected in their patch front dynamics which do not differ from the ecology control in Fig. 3.3-A. Initial patch front speeds as observed in Fig. 3.3-B do not seem to differ qualitatively from the ecology control patch front speeds for the MMRT model and with slower hot patch front speeds for the EAAR model.

As observed in Fig. 3.2 - G, for the MMRT model the TPC may widen by changing the heat capacity as it changes the sensitivity of enthalpy change and entropy change to

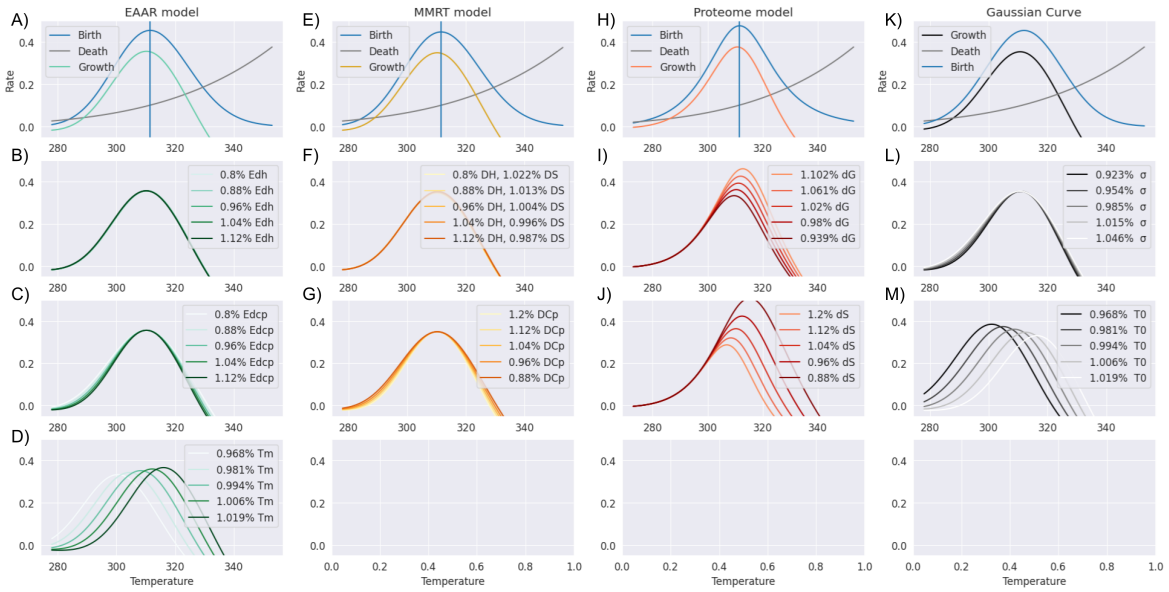


Figure 3.2: For the 4 considered model: Proteome model (Eqn. 1.7), MMRT model (Eqn. 1.22), EAAR model (Eqn. 1.23) and the Gaussian curve, average TPCs with rate on the y-axis and temperature on the x-axis that is used to initialise respective simulations are shown along with effect of respective parameter variation. Row EAAR model A): Birth, death and growth rate as functions of temperature; B): Effect of variation in enthalpy of folding the enzymes; C): Effect of variation in entropy of folding the enzymes; D): Effect of variation in heat capacity of folding the enzymes on the TPC. Row MMRT model E): Birth, death and growth rate as functions of temperature; F): Effect of variation in enthalpy change at 20 C; G): Effect of variation in entropy change at 20 C; Row Proteome model H): Birth, death and growth rate as functions of temperature; I): Effect of variation in activation energy of denaturation at 20 C; J): Effect of variation in entropy change of denaturation at 20 C.; Row Gaussian curve K): Birth, death and growth rate as functions of temperature; L): Effect of variation in standard deviation of curve; M): Effect of variation in mean of the curve. Parameters are varied about their mean, within the standard deviations of its mutation kernel.

temperature, or shift its peak upwards and rightwards with decreased growth at colder temperatures, due to the assumed Enthalpy-Entropy compensation. From Fig. 3.4 the TPC seems to adapt by broadening its curve at the cold patch front and the hot patch front does not seem different from its burn-in TPC. The trend is confirmed in patch front dynamics of the evolving traits at the hot patch front stay the same throughout the expansion while the mean of the traits of the cold patch front change from its initial value as seen in Fig. 5.2. There is high overlap in the inter-quartile ranges of the trait means and there is significant difference in hot and cold patch front traits for heat capacity changes only.

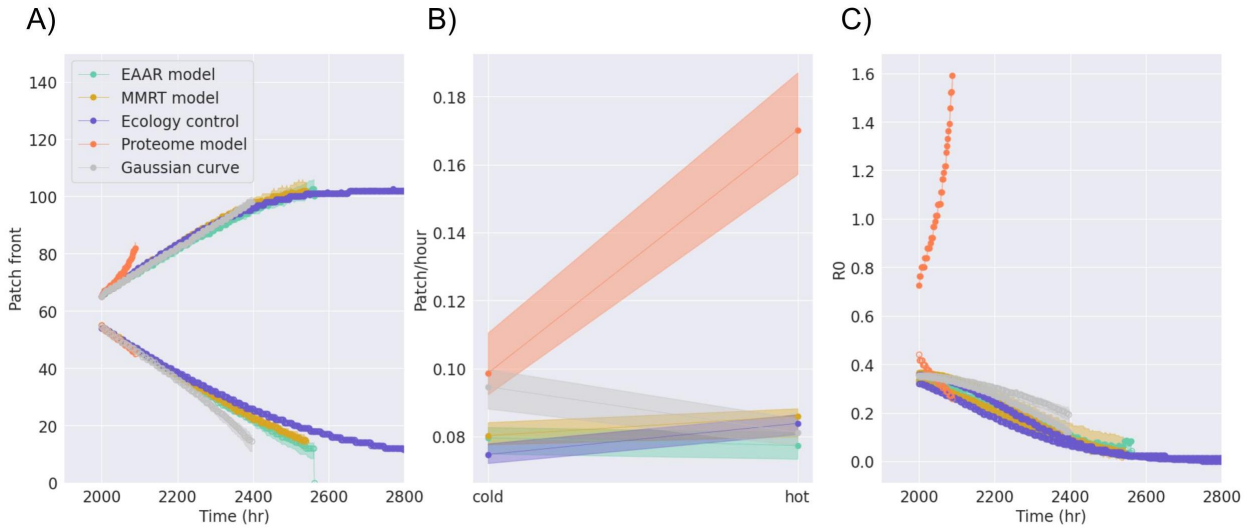


Figure 3.3: Range front dynamics from simulations with local adaptation and no dispersal evolution. Patch front and their properties are averaged across 40 replicates. At every 2 hours, the last 3 occupied patches with more than 10 individuals are considered as patch front. A): Patch front which is the furthest occupied patch versus time in hours; Panel B: Initial speeds of expansion at the cold and hot patch front calculated by fitting a linear curve to patch front dynamics versus time for time ¡ 2100 hours; Panel C: Growth rate from respective TPCs versus time calculated using traits at each patch front and patch temperature.

The EAAR model, despite being mathematically similar to the MMRT model, is more flexible within the assumed mutation kernel due to consideration of the enzyme melting temperature. Changing the melting temperature of the enzyme, practically shifts the curve to a new optimum and displays a 'hotter is better' trend. Trait patterns in Fig. 5.3 reflect the same; the only significant difference in hot versus cold trait is for the melting temperature. But it does not change the patch front speed significantly. For both the models, looking at Fig. 3.3-C, growth rate at the hot front increases with time and the within population inter-quartile ranges for all the traits in Fig. 5.2 and Fig. 5.3 increase near the end of the landscape. This could imply that the mutation kernel assumed is too narrow or a longer landscape is required.

Last, for the traditionally assumed Gaussian TPC, the cold patch-front speed is higher than in the other scenarios. This is due to the 'colder is better' trend shown by the Gaussian curve as seen in Fig. 3.2 - L M where shift in the mean leads to a reduced optimal growth rate while the effect of widening the curve is dampened at the hot end. Also the trend is

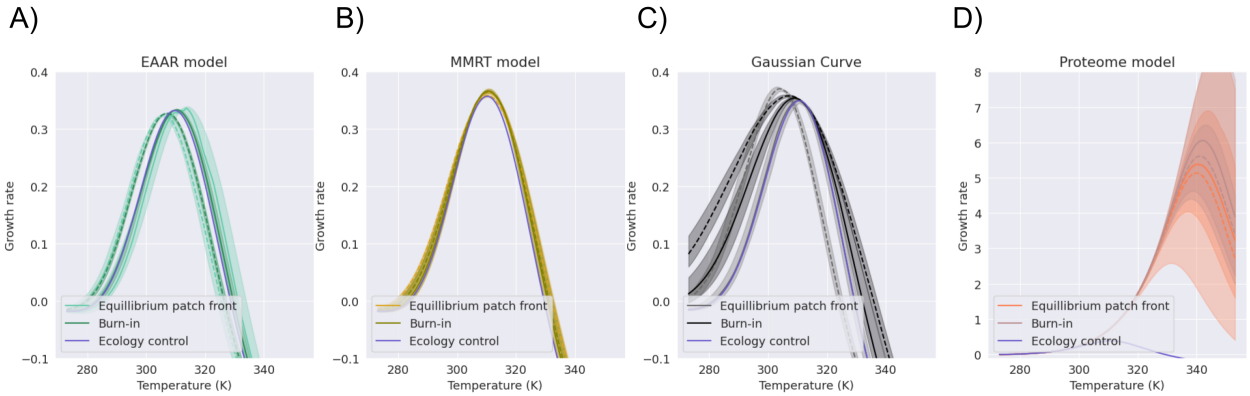


Figure 3.4: Comparison of TPCs at different time points in the simulations without dispersal evolution. For all panels A-D): Purple curve is the ecological control without dispersal evolution and local adaptation. The dotted lined TPC is the TPC for the cold patch front and solid lined TPC is for the hot patch front. Light colored TPC is the equilibrium TPC at the end of the burn-in and the darker colored TPCs are equilibrium TPC at the end of the simulation which is reached when the first replicate reaches either end of the landscape. To plot the TPCs, patch front trait values were calculated by averaging the median trait values in the last 3 occupied patches with more than 10 individual at respective patch fronts. The IQR of the curves were calculated by measuring the IQR of growth rates for the TPC for each replicate, at discrete range of temperatures.

seen in the Fig. 3.3-C as the cold patch front growth rate is faster than the hot patch front growth rate. The symmetric change in Gaussian Curve when its mean and variance are varied, cannot track the exponential increase in death rate which is unlike enzyme melting temperature in the EAAR model that can also shift the optimum of the curve almost linearly.

### 3.2.2 Local adaptation with dispersal evolution

Next I introduce the evolution of the emigration trait during range expansion. The ecology control in this case has dispersal evolution without local adaptation. Dispersal evolution makes individuals, including in the ecology control to Fig. 3.5-A reach the end of the landscape on the cold side. However, individuals cannot survive beyond patch 10, because of high stochasticity at the patch front. This implies that sinks are being created at either ends of the landscape. Overall the differences between models decreased as they reach the end of the landscape much faster.

The dispersal trait evolves to almost a magnitude higher than the starting value and it leads to a lot of gene flow for the local adaptation traints as can be seen in Fig. 5.5-5.8 as well as in Fig. 3.6 where equilibrium TPC are intermediates of the cold and hot patch front TPCs after burn-in.

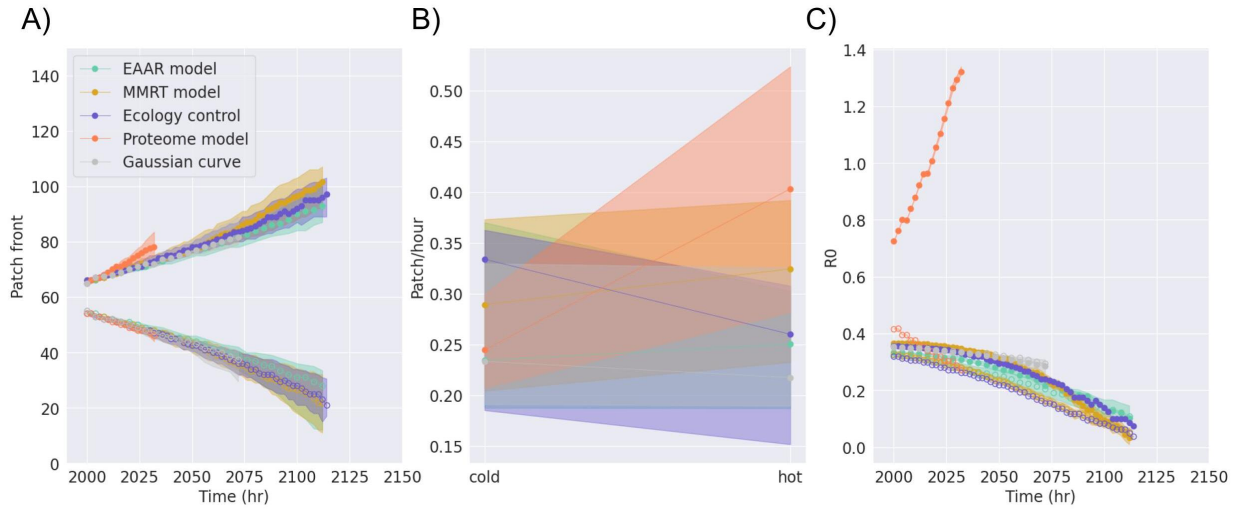


Figure 3.5: Range front dynamics from simulations with local adaptation and dispersal evolution are shown. Patch front and their properties are averaged across 40 replicates. At every 2 hours, the last 3 occupied patches with more than 10 individuals are considered as patch front. A): Patch front which is the furthest occupied patch versus time in hours; Panel B: Initial speeds of expansion at the cold and hot patch front calculated by fitting a linear curve to patch front dynamics versus time for time ¡ 2100 hours.; Panel C: Growth rate from respective TPCs versus time calculated using traits at each patch front and patch temperature.

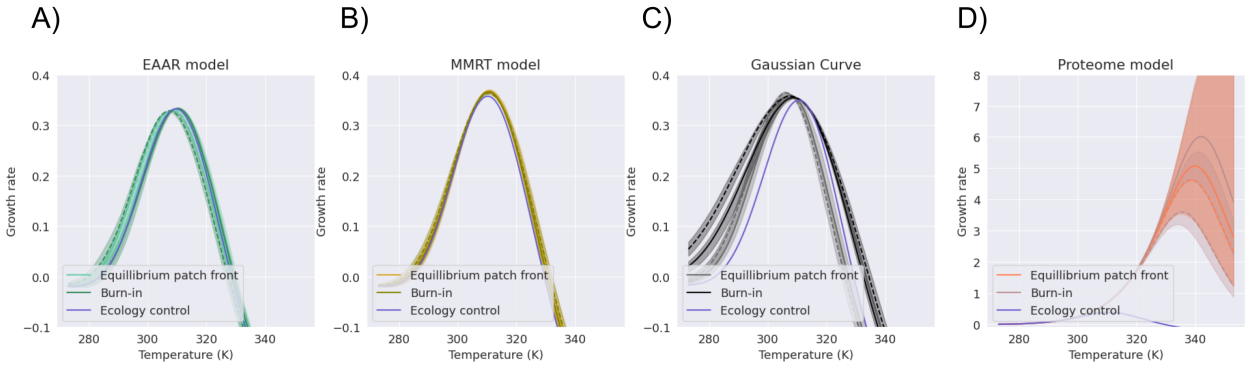


Figure 3.6: Comparison of TPCs at different time points in the simulations with dispersal evolution. For all panels A-D): Purple curve is the ecological control with dispersal evolution and no local adaptation. The dotted lined TPC is the TPC for the cold patch front, and solid lined TPC is for the hot patch front. Light colored TPC is the equilibrium TPC at the end of the burn-in and the darker colored TPCs are equilibrium TPC at the end of the simulation which is reached when the first replicate reaches either end of the landscape. To plot the TPCs, patch front trait values were calculated by averaging the median trait values in the last 3 occupied patches with more than 10 individual at respective patch fronts across 40 replicates. The IQR of the curves were calculated by measuring the IQR of growth rates for the TPC for each replicate, at discrete range of temperatures.

# Chapter 4

# Discussion

I studied a comprehensive set of mechanistic models describing TPCs with an evolutionary framework during range expansions across a temperature gradient. Importantly, I consider mechanisms at the molecular level behind thermal adaptation and show how these microscopic assumptions cascade up to impact large scale patterns such as range expansion dynamics. I have identified three models from literature: Proteome model (Eqn. 1.7), MMRT model (Eqn. 1.22) and EAAR model (Eqn. 1.23) that represent different mechanisms. I primarily consider protein thermal stability adaptation through the Proteome Model (Eqn. 1.7). I consider evolution of enzyme catalysis through the Macromolecular Rate Theory (Eqn. 1.22). Finally I combine the two in the Enzyme Activated Arrhenius Rate theory (Eqn. 1.23) which proposes a functional form for effect of enzyme denaturation on enzyme catalysis.

In addition to my theoretical work, I have confronted the different models with empirical data from protist microcosms. The differences among the models were reflected in their fit in Fig. 3.1. I find support for the Proteome model in 2 replicates and the EAAR model in 1 replicate. It is difficult to comment on underlying mechanisms from the fit, especially because the small number of data points leads to high Pareto k values.

Regardless of selected model, I find that assumption of thermal scaling of the feeding rate in the Beverton-Holt model leads to asymmetry in carrying capacity in hot and cold patches in Fig. 2.1. From simulations, with the Proteome model, when protein stability does not have genetic constrains to evolve and is the limiting condition for thermal evolution,

one would predict rapid evolution to hot patches and accelerated patch front expansion. There is not much difference among the range dynamics of EAAR and MMRT models. The Gaussian curve shows a 'colder is better' trend as the maximum growth rate decrease with increase in optimum temperature due to the exponentially increasing death rate, hence it ends up showing faster cold patch front speed than hot patch front speed. Despite the same exponentially scaling death rate assumption and almost symmetrical growth curves for the other models (except the Proteome model), changes in their parameters were asymmetrical i.e when optimal temperature is shifted to higher temperatures, the increase in optimal birth rate is more than the increase in death rate at the new optimal temperature. If the adapting TPC is not able to compensate it leads to a 'colder is better' dynamics observed for the Gaussian curve. Hence, asymmetry in the functional form and fitness effect of the adapting parameters is shown to be important in assumed TPC curves.

### 4.0.1 Empirical observations

Metabolic rate is dependent on environmental factors and variation of metabolic reaction norms have been observed widely across latitudes for ectotherms [109, 59, 95]. For example, in a study by White et al. [109] they analysed a data-set for fishes where metabolic rate and citrate synthase activity is found to be higher for inidivudals from colder latitutudes compared to hotter latitudes at intermediate temperatures. But when absolute activity at their habitat temperatures are measured cold adapted species have lower metabolic rates. I find support for this behaviour in the EAAR and MMRT models where below the peak temperatures, the cold adapted TPCs have higher growth rate than the hot adapted TPC but since the above studies do not measure the whole TPC it is difficult to provide the models as possible mechanisms. Further, intraspecific variations in metabolic enzymes along latitudinal gradients in some insects have been attributed to thermal evolution [80, 57, 95] and is reviewed in [13]. For example, extensive work has been done on the PGI (phosphoglucose isomerase). Isoforms of the enzyme with higher activity are shown to be less thermally stable while low-activity isoforms are more thermally stable [95]. In Glanville butterflies, the enzyme property has been shown to affect flight capacity as it affect how fast their flight muscles can be warmed. Early oviposition of Glanville butterflies with heterozygous PGI isoforms occurs as they can fly at lower temperatures and has been shown to increase clutch size [87]. But homozygous isoforms are shown to be better for extreme temperature evolu-

tion and distribution of PGI genotypes among natural populations correlates with habitat temperature [95]. The PGI enzyme shows a thermal stability - kinetic efficiency trade off. The explanations provided for thermal-stability - kinetic efficiency trade offs is often that changes needed to increase protein thermal stability make the enzyme more inflexible hence reducing activity at colder temperatures. Though the models I consider do not encode the phenomena explicitly, by assuming the Enthalpy-Entropy compensation in MMRT model, I get a similar trend. The hot adapted mean TPC in Fig. 3.3 is narrower but with a higher rate peak compared to its cold adapted patch front. In MMRT model, I do not consider thermal stability, but it could be that thermal stability is correlated with enthalpic changes occurring during enzyme-substrate reactions. These differences in thermal tolerances play an important role in invasion success of novel species. Better cold adaptation has been key to the widespread invasion of the redback spider [72] and the woolly hemlock adelgid [17].

Stronger correlation is found between minimum lethal temperature and ambient temperature compared to maximum lethal temperature and ambient temperature. Hence colder tolerances have been thought to be more evolutionary labile than heat tolerance. The asymmetry results from limited variation in organisms to compensate for protein denaturation and membrane disruption[6]. Heat shock proteins have been shown not to change heat tolerance but just avoid aggregation of denatured protein [55]. Rapid evolution to colder regimes has been documented in damselflies with increased niche breadth at colder patch fronts due thermal release of the heat tolerance [62, 19]. Further cold-adapted damsel flies have higher developmental rate at hotter temperatures as well, as seen in the Proteome model. My results may be suggesting better evolution to colder temperatures as burn-in TPCs seem more shifted than their ecological controls. Density effects due to the asymmetry in carrying capacity may be underlying the phenomena and may be worth looking into.

### 4.0.2 Effect of temperature fluctuations

Climate change is predicted to bring higher temperatures but also widely erratic climate [103, 8]. Additionally, latitudinal clines observed for metabolic properties don't necessarily need to correlate with mean temperatures as temperature fluctuations are increase with increase in latitudes [109]. Effect of temperature fluctuations are translated to fitness effects depending on the TPC's skewness. High variation in environmental temperature near optimum temperature of TPC reduces the peak performance temperature as temperatures

above the optimum temperatures lead to a sharp decrease in fitness. While high variation in environmental temperatures colder than the optimal temperature would increase the peak performance due to the sharp rise of the TPC [103]. Hence, different mechanisms of TPC evolution as in our models would lead to different effects of temperature fluctuations,such as the rapid acceleration of the Proteome model into hot patches may not be as rapid if temperature fluctuations were also increasing with mean temperature. On the other hand it would make cold adaptation even faster. This could be an interesting study in the future.

### 4.0.3 Sensitivity to dispersal rates

TPC describes the plastic phenotypic response of an individual to temperature. Phenotypic plasticity could reduce the effect of environmental shift letting the population persist for longer and can both speed up or slow down genetic change [78]. Effect of phenotypic plasticity in evolutionary rescue has been theorised to be dependent on the cost of plasticity [89]. Low costs, high migration and environmental heterogeneity could select for high phenotypic plasticity [100] so it may be interesting to look at sensitivity of the results to dispersal rates in the absence of dispersal evolution. High dispersal rates due to dispersal evolution also lead to a lot more mixing as can be seen in the adapting trait dynamics in Fig. 5.5 - 5.8 for all cases where trait means converge. In case of a sexual reproduction model it could lead to a high genetic load if hot and cold adapted individuals will reproduce more often to generate sub-optimal phenotype.

### 4.0.4 Shortcomings

I conduct my simulations with a single parameter set and landscape properties. I need to check the robustness of my results with sensitivity analysis on landscape length and gradient steepness, as well as different initial TPCs. A longer landscape is required to understand effect of dispersal evolution more as the evolving dispersal traits makes range front speed very fast. In several cases, patch front traits do not seem to differ from those at the end of the burn in and IQR of the trait within the patch population of the of all adapting traits drops to zero during range expansion which seems to suggest almost a single genotype is expanding till the border of its TPC and then increase in population IQR of all adapting traits is seen near the end of the landscape. Alternatively, changes can be made for initialised TPC to

be narrower. Finally, I stop my simulations when the first replicate reaches the end of the landscape and only consider the dynamics during range expansion and not at stationary state. But it would be interesting to study the spatial distribution of the traits after all patches have reached their equilibrium and effect of the asymmetry in carrying capacity across the landscape in Fig. 2.2.

My study takes into consideration protein level properties and associated trade offs which have been empirically observed from my limited literature review. I consider effect of temperature on stability of enzymes and their reaction rates separately. As pointed out by the authors of Hobbs et al. [51], for a complete picture, it will be important to combine the two phenomena. Additionally, it is important to consider that substrate is limited in real systems and substrate binding or the Michealis constant $K_m$ has been widely shown to demonstrate thermal evolution [92]. It could also allow one to look into effect of the flexibility-stability trade off hypothesis [68, 36] where hotter adapted enzymes lack flexibility which reduces catalytic efficiency. Possible way to include evolution of $K_m$ could be to establish a relation between reduced flexibility of enzymes that would affect the heat capacity difference of enzyme catalysis and thermostability of enzymes. Apart from changes in properties of enzymes, general responses to temperature stress can be changes in enzyme concentration and modification to membrane properties and intracellular environment which can be induced by genotypic changes or acclimation [21, 52].

Observations of latitudinal cline of enzyme properties are usually studies on a single enzyme or protein and though they provide correlation between organism fitness and enzyme function, they need to be put in context of the complex ecosystem that individuals interact with. Since selection acts on functional phenotype, trade offs I consider in my project will not translate to higher levels of organisation such as population growth rate as I have assumed. Trade offs in traits more closely related to fitness need to be considered. Growth rates are often more constrained by resource limitations and higher foraging rates would come at the higher risk of predation [108]. Additionally in organisms with more complex life histories, one can have trade offs between faster developmental rate and size [22] and more energy allocation to growth rate could decrease reproductive output [77]. Our results hence hold for limited cases of ectotherms when thermal evolution is limited by protein properties and functional forms of TPC for protein reaction rates can translate to population growth rates. But it is unlikely that the a TPC is going to follow a single biochemical process as many reactions are involved in metabolic pathway and there are probably different biphysical

constraints across the thermal range like at extreme high and low temperatures [91].

### 4.0.5 Conclusion

In my study I consider three different mechanisms, but as discussed in the Literature review, pervasive epistasis can severely restrict the trajectories that protein evolution can take [47]. Therefore it is difficult to apply the models generally or assume they form an exhaustive set of mechanisms. I instead hope to show that assumptions of different mechanism defining the TPC will constrain how the TPC would change in response to temperature gradients. Apart from the shape of the curve, it becomes important to consider the effect of variation of the evolving parameters. Despite starting with almost the same TPCs when different protein level properties are under selection, they can show very different range dynamics. Further, I find that, generally, if intraspecific competition scales with birth rate as I assume, carrying capacity will be decrease with temperatures. Consequences of the same need to be studies further. Hence, integration of explicit mechanisms shaping TPCs and constraining its evolution could lead to more insights into the eco-evolutionary feedback of thermal evolution.

# Chapter 5

# Supplementary Material

## 5.1 Supplementary Figures

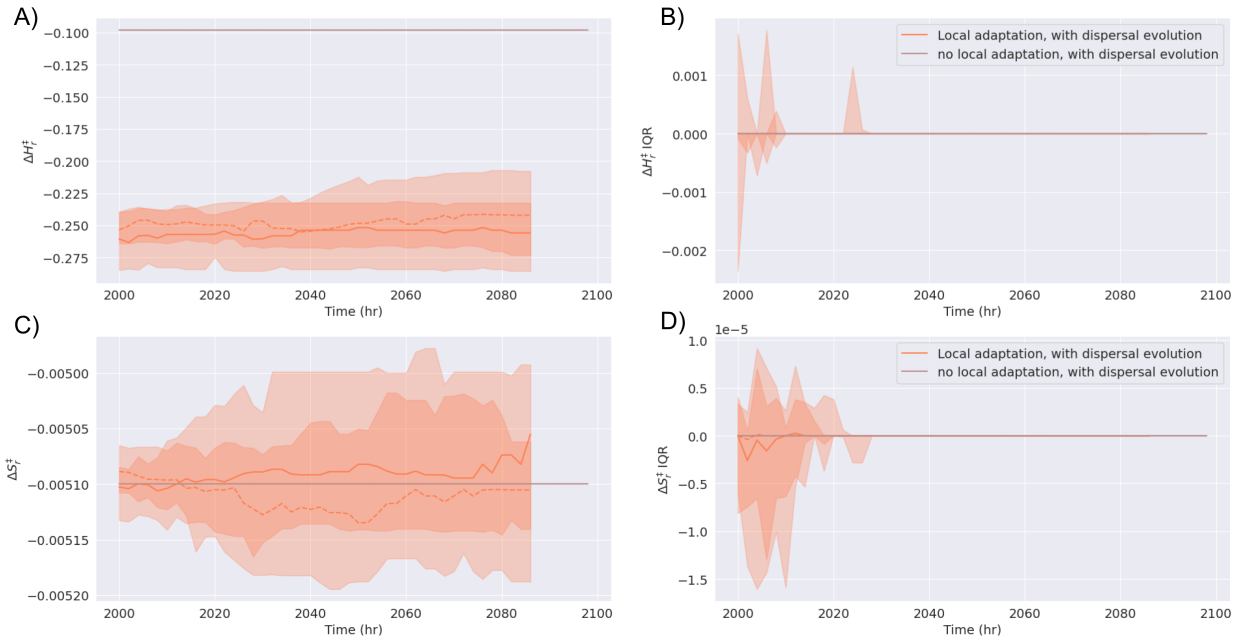


Figure 5.1: Comparison of average evolving trait value, its population level variation and among replicate variation. At every 2 hours simulation time, median and IQR of the evolving trait values of the last 3 occupied patches with more than 10 individuals across 40 replicates are averaged, for simulations without dispersal evolution of the Proteome model. Adapting parameters are $\Delta G_r$: Activation free energy for denaturation at reference temperature, $\Delta S_r$: Activation entropy for denaturation at reference temperature. Panel A): Median of $\Delta G_r$ trait with IQR for among replicates variation; Panel B): Median of patch population level IQR of $\Delta G_r$ trait with IQR for among replicates; Panel C): Median of $\Delta S_r$ trait with IQR for among replicates variation; Panel D): Median of patch population level IQR of $\Delta S_r$ trait with IQR for among replicates.

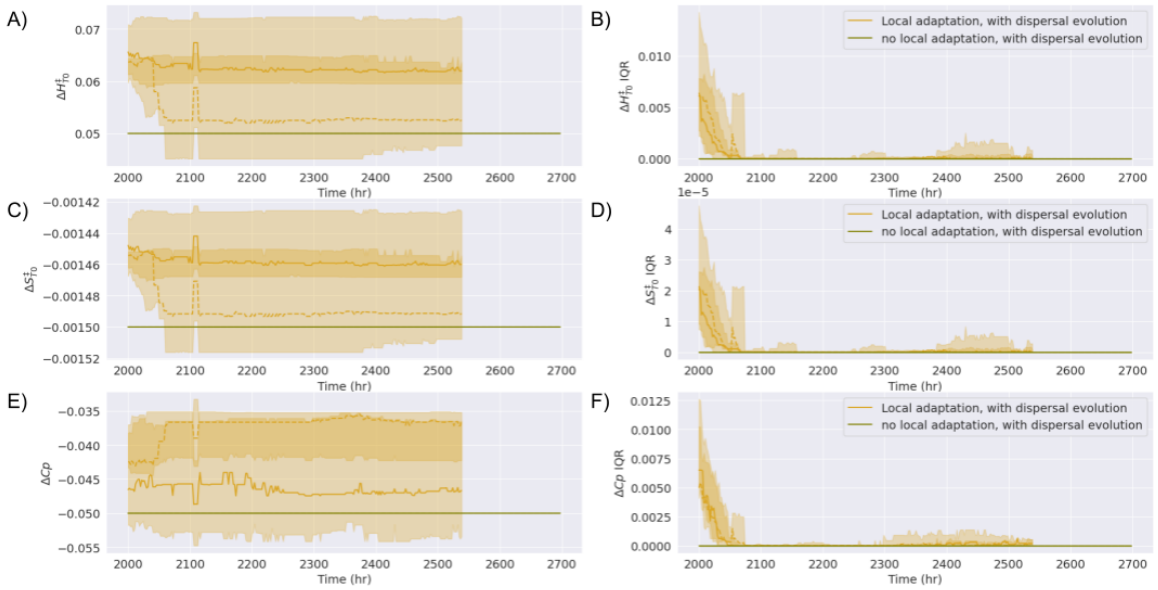


Figure 5.2: Comparison of average evolving trait value, its population level variation and among replicate variation. At every 2 hours simulation time, median and IQR of the evolving trait values of the last 3 occupied patches with more than 10 individuals across 40 replicates are averaged, for simulations without dispersal evolution of the MMRT model. Adapting parameters are $\Delta H^{\ddagger}_{T_0}$:Enthalpy change at reference temperature, $\Delta S^{\ddagger}_{T_0}$: Entropy change at reference temperature, $\Delta C_p$: Heat capacity difference. Panel A): Median of $\Delta H^{\ddagger}_{T_0}$ trait with IQR for among replicates variation; Panel B): Median of patch population level IQR of $\Delta H^{\ddagger}_{T_0}$ trait with IQR for among replicates; Panel C): Median of $\Delta S^{\ddagger}_{T_0}$ trait with IQR for among replicates variation; Panel D): Median of patch population level IQR of $\Delta S^{\ddagger}_{T_0}$ trait with IQR for among replicates; Panel E): Median of $\Delta C_p$ trait with IQR for among replicates variation; Panel F): Median of patch population level IQR of $\Delta C_p$ trait with IQR for among replicates.

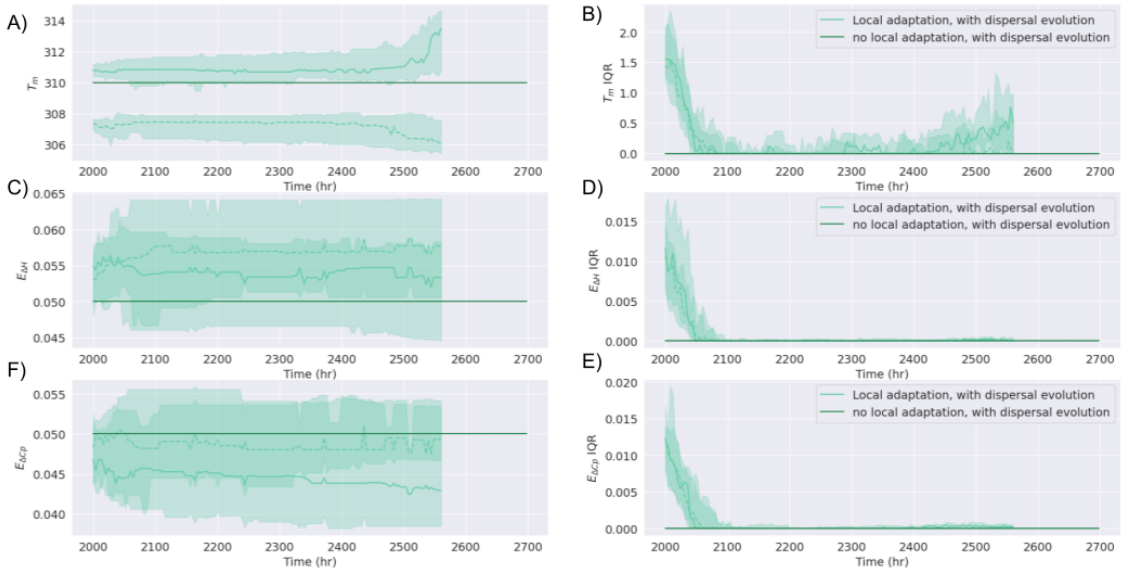


Figure 5.3: Comparison of average evolving trait value, its population level variation and among replicate variation. At every 2 hours simulation time, median and IQR of the evolving trait values of the last 3 occupied patches with more than 10 individuals across 40 replicates are averaged, for simulations without dispersal evolution of the EAAR model. Adapting parameters are $E_{\Delta H}$: Lowered activation energy wrt $\Delta H$ , $T_m$: Enzyme melting temperature, $E_{\Delta C_p}$: Lowered activation energy wrt $\Delta C_p$; Panel A): Median of $T_m$ trait with IQR for among replicates variation; Panel B): Median of patch population level IQR of $T_m$ trait with IQR for among replicates; Panel C): Median of$E_{\Delta H}$ trait with IQR for among replicates variation; Panel D): Median of patch population level IQR of$E_{\Delta H}$ trait with IQR for among replicates; Panel E): Median of $E_{\Delta C_p}$ trait with IQR for among replicates variation; Panel F): Median of patch population level IQR of $E_{\Delta C_p}$ trait with IQR for among replicates.

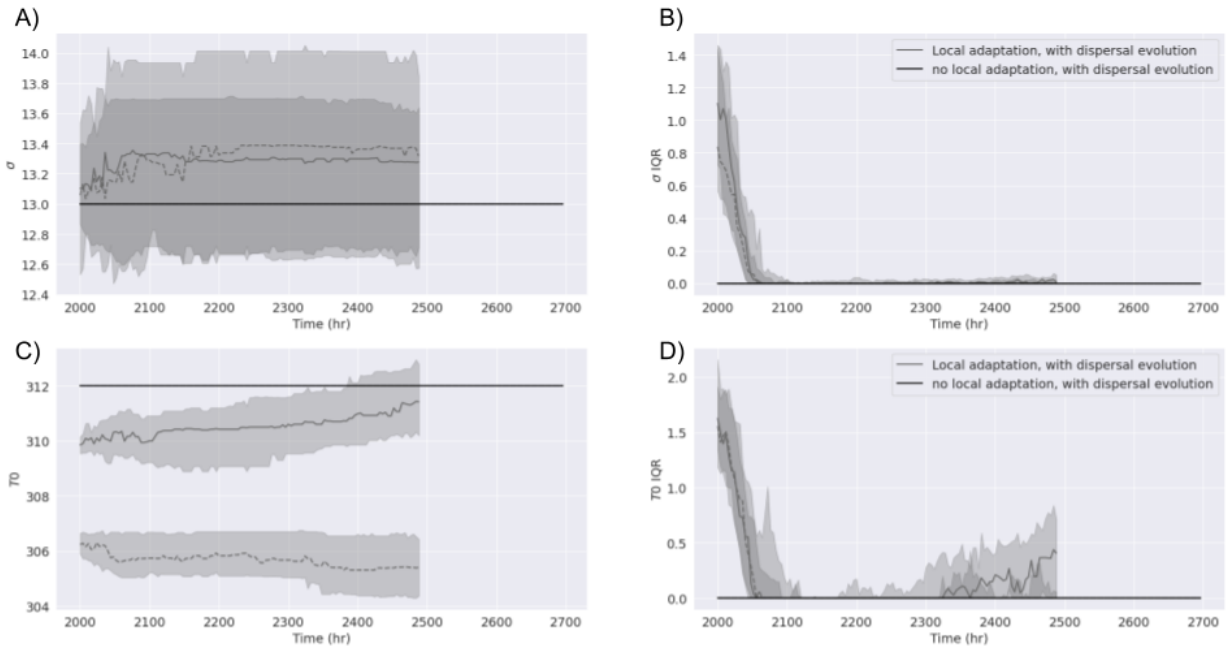


Figure 5.4: Comparison of average evolving trait value, its population level variation and among replicate variation. At every 2 hours simulation time, median and IQR of the evolving trait values of the last 3 occupied patches with more than 10 individuals across 40 replicates are averaged, for simulations without dispersal evolution of the Gaussian curve model. Adapting parameters are $\sigma$: Standard deviation of the curve, $T_0$: Mean of curve; Panel A): Median of $\sigma$ trait with IQR for among replicates variation; Panel B): Median of patch population level IQR of $\sigma$ trait with IQR for among replicates; Panel C): Median of $T_0$ trait with IQR for among replicates variation; Panel D): Median of patch population level IQR of $T_0$ trait with IQR for among replicates.

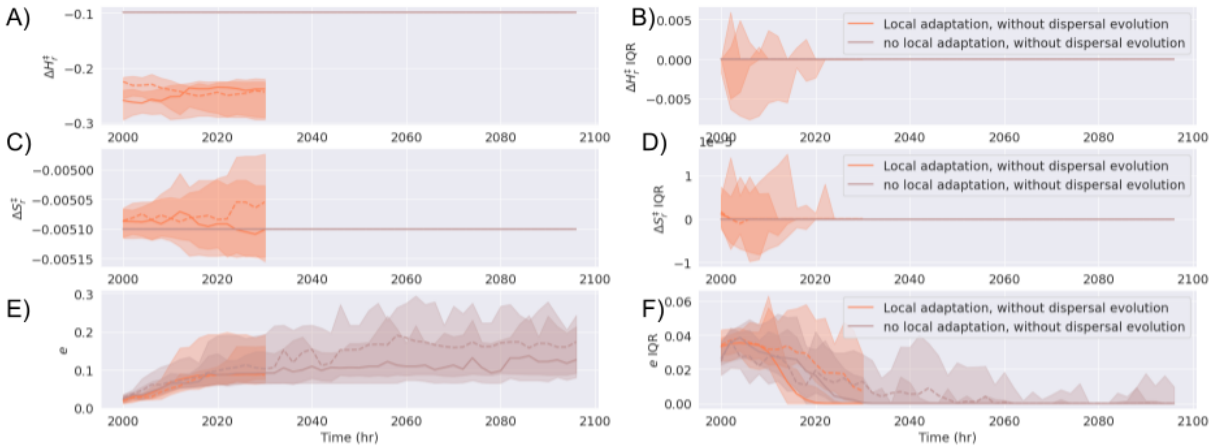


Figure 5.5: Comparison of average evolving trait value, its population level variation and among replicate variation. At every 2 hours simulation time, median and IQR of the evolving trait values of the last 3 occupied patches with more than 10 individuals across 40 replicates are averaged, for simulations with dispersal evolution of the Proteome model. Adapting parameters are $\Delta G_r$: Activation free energy for denaturation at reference temperature, $\Delta S_r$: Activation entropy for denaturation at reference temperature, $e$: Dispersal trait; Panel A): Median of $\Delta G_r$ trait with IQR for among replicates variation; Panel B): Median of patch population level IQR of $\Delta G_r$ trait with IQR for among replicates; Panel C): Median of $\Delta S_r$ trait with IQR for among replicates variation; Panel D): Median of patch population level IQR of $\Delta S_r$ trait with IQR for among replicates; Panel E): Median of $e$ trait with IQR for among replicates variation; Panel F): Median of patch population level IQR of $e$ trait with IQR for among replicates.

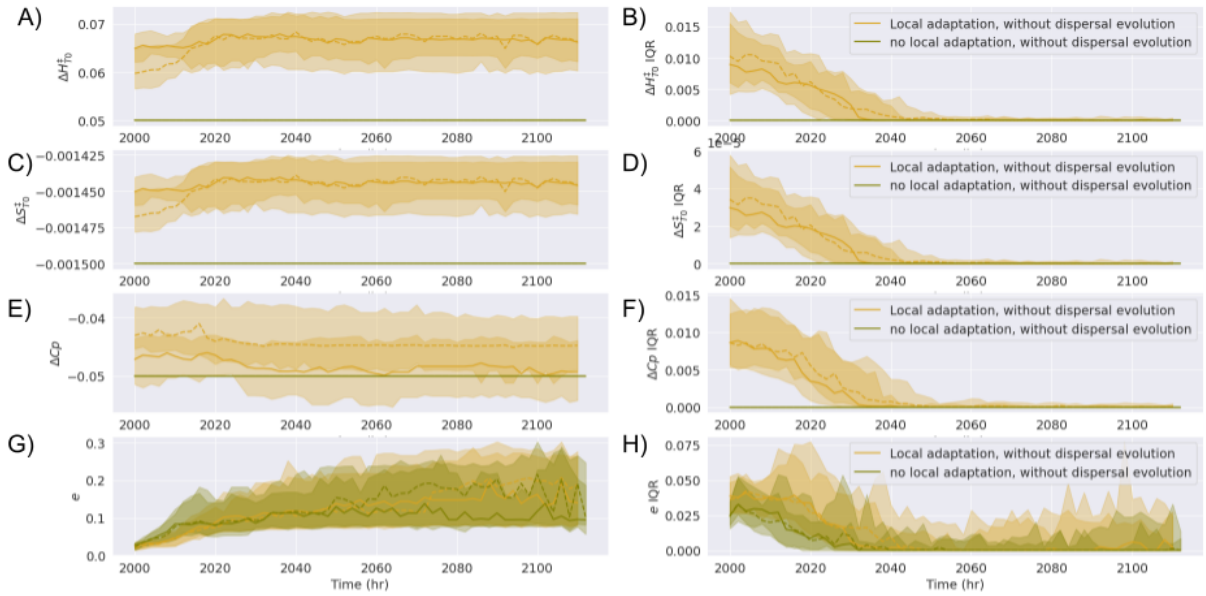


Figure 5.6: Comparison of average evolving trait value, its population level variation and among replicate variation. At every 2 hours simulation time, median and IQR of the evolving trait values of the last 3 occupied patches with more than 10 individuals across 40 replicates are averaged, for simulations with dispersal evolution of the MMRT model. Adapting parameters are $\Delta H^{\ddagger}_{T_0}$:Enthalpy change at reference temperature, $\Delta S^{\ddagger}_{T_0}$: Entropy change at reference temperature, $\Delta C_p$: Heat capacity difference , $e$: Dispersal trait; Panel A): Median of $\Delta H^{\ddagger}_{T_0}$ trait with IQR for among replicates variation; Panel B): Median of patch population level IQR of $\Delta H^{\ddagger}_{T_0}$ trait with IQR for among replicates; Panel C): Median of $\Delta S^{\ddagger}_{T_0}$ trait with IQR for among replicates variation; Panel D): Median of patch population level IQR of $\Delta S^{\ddagger}_{T_0}$ trait with IQR for among replicates; Panel E): Median of $\Delta C_p$ trait with IQR for among replicates variation; Panel F): Median of patch population level IQR of $\Delta C_p$ trait with IQR for among replicates; Panel E): Median of $e$ trait with IQR for among replicates variation; Panel F): Median of patch population level IQR of $e$ trait with IQR for among replicates.

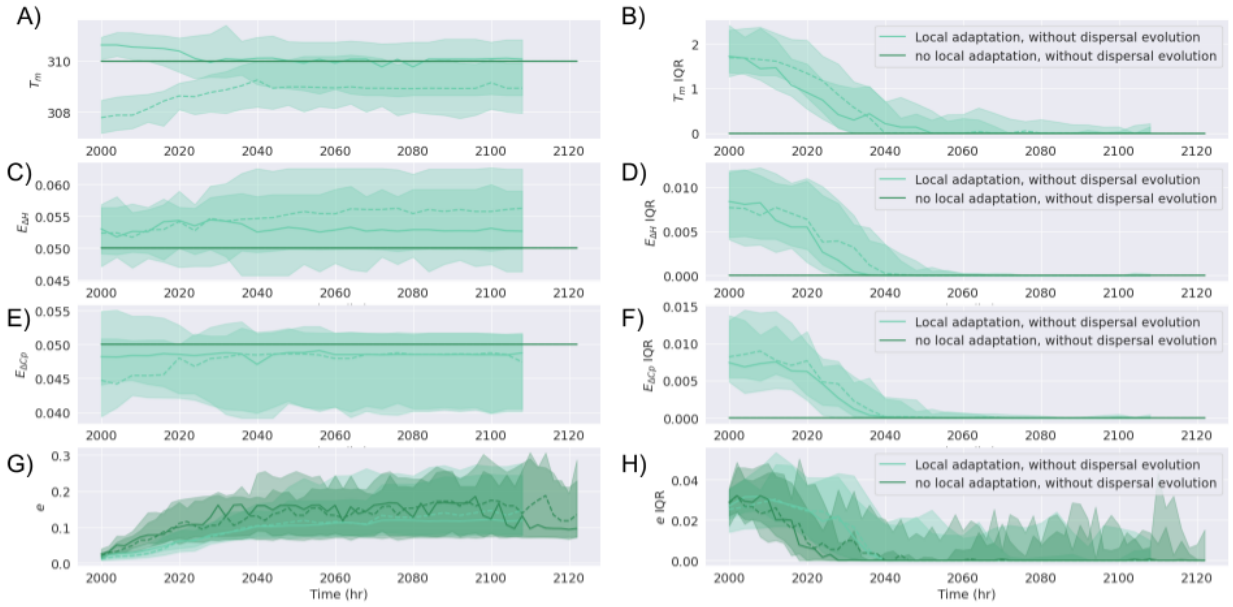


Figure 5.7: Comparison of average evolving trait value, its population level variation and among replicate variation. At every 2 hours simulation time, median and IQR of the evolving trait values of the last 3 occupied patches with more than 10 individuals across 40 replicates are averaged, for simulations with dispersal evolution of the EAAR model. Adapting parameters are $E_{\Delta H}$: Lowered activation energy wrt $\Delta H$ , $T_m$: Enzyme melting temperature, $E_{\Delta C_p}$: Lowered activation energy wrt $\Delta C_p$, $e$: Dispersal trait; Panel A): Median of $T_m$ trait with IQR for among replicates variation; Panel B): Median of patch population level IQR of $T_m$ trait with IQR for among replicates; Panel C): Median of $E_{\Delta H}$ trait with IQR for among replicates variation; Panel D): Median of patch population level IQR of $E_{\Delta H}$ trait with IQR for among replicates; Panel E): Median of $E_{\Delta C_p}$ trait with IQR for among replicates variation; Panel F): Median of patch population level IQR of $E_{\Delta C_p}$ trait with IQR for among replicates; Panel E): Median of $e$ trait with IQR for among replicates variation; Panel F): Median of patch population level IQR of $e$ trait with IQR for among replicates.

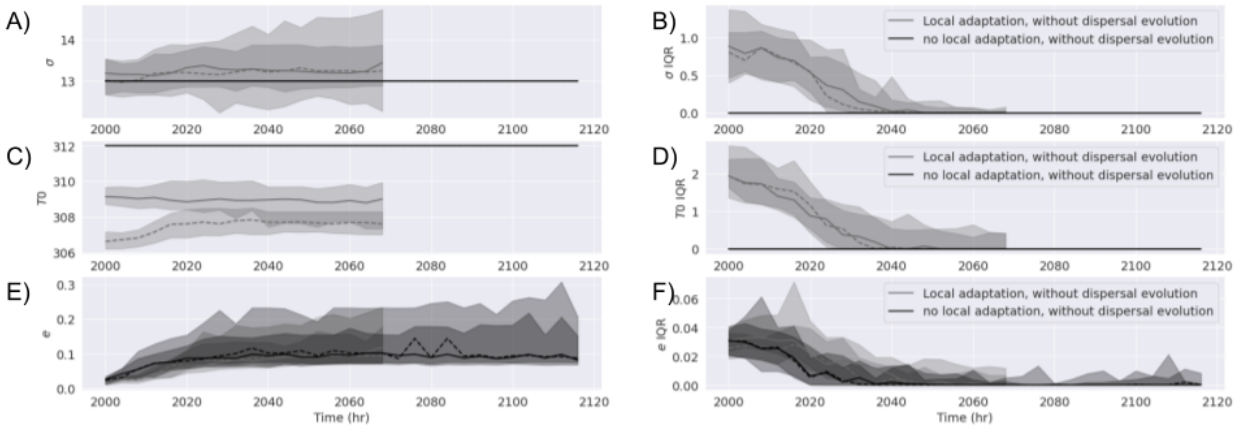


Figure 5.8: Comparison of average evolving trait value, its population level variation and among replicate variation. At every 2 hours simulation time, median and IQR of the evolving trait values of the last 3 occupied patches with more than 10 individuals across 40 replicates are averaged, for simulations with dispersal evolution of the Gaussian curve model. Adapting parameters are $\sigma$: Standard deviation of the curve, $T_0$: Mean of curve, $e$: Dispersal trait; Panel A): Median of $\sigma$ trait with IQR for among replicates variation; Panel B): Median of patch population level IQR of $\sigma$ trait with IQR for among replicates; Panel C): Median of $T_0$ trait with IQR for among replicates variation; Panel D): Median of patch population level IQR of $T_0$ trait with IQR for among replicates; Panel E): Median of $e$ trait with IQR for among replicates variation; Panel F): Median of patch population level IQR of $e$ trait with IQR for among replicates.

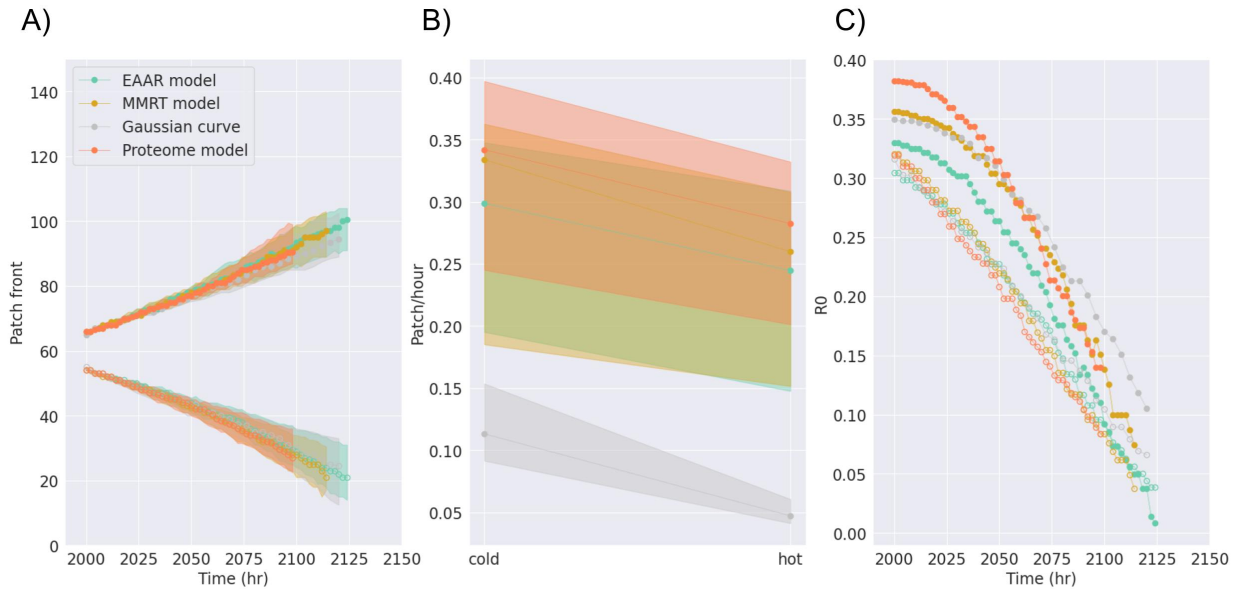


Figure 5.9: Range front dynamics from simulations with local adaptation and without dispersal evolution are shown. Patch front and their properties are averaged across 40 replicates. At every 2 hours, the last 3 occupied patches with more than 10 individuals are considered as patch front. A): Patch front which is the furthest occupied patch versus time in hours; Panel B: Initial speeds of expansion at the cold and hot patch front calculated by fitting a linear curve to patch front dynamics versus time for time ¡ 2100 hours.; Panel C: Growth rate from respective TPCs versus time calculated using traits at each patch front and patch temperature.

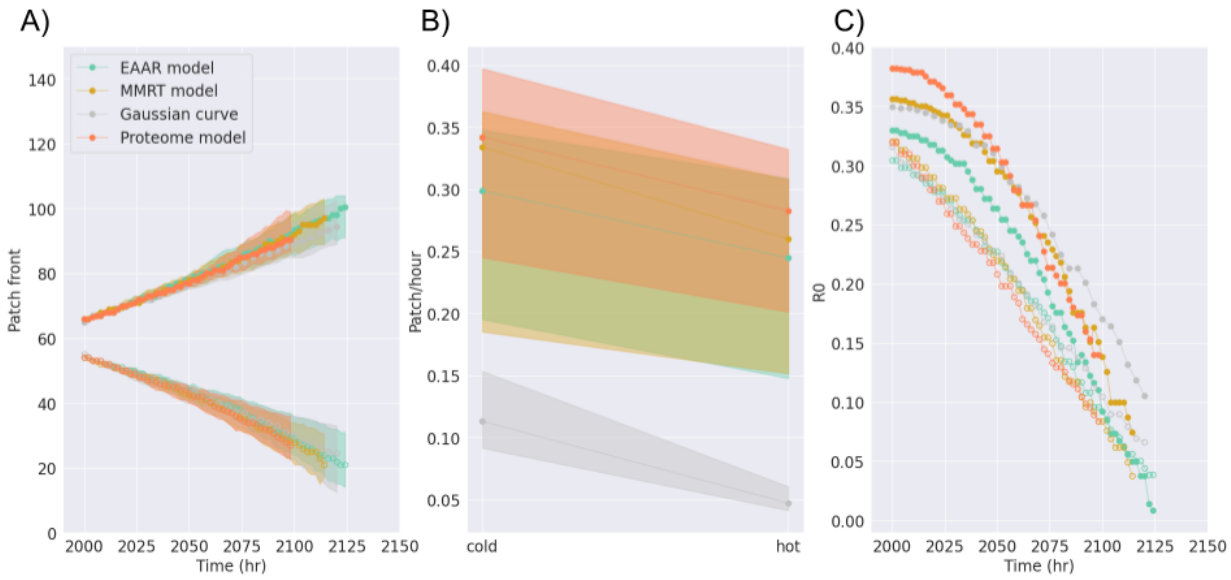


Figure 5.10: Range front dynamics from simulations with local adaptation and dispersal evolution are shown for all the ecology controls. Patch front and their properties are averaged across 40 replicates. At every 2 hours, the last 3 occupied patches with more than 10 individuals are considered as patch front. A): Patch front which is the furthest occupied patch versus time in hours; Panel B: Initial speeds of expansion at the cold and hot patch front calculated by fitting a linear curve to patch front dynamics versus time for time ¡ 2100 hours.; Panel C: Growth rate from respective TPCs versus time calculated using traits at each patch front and patch temperature.

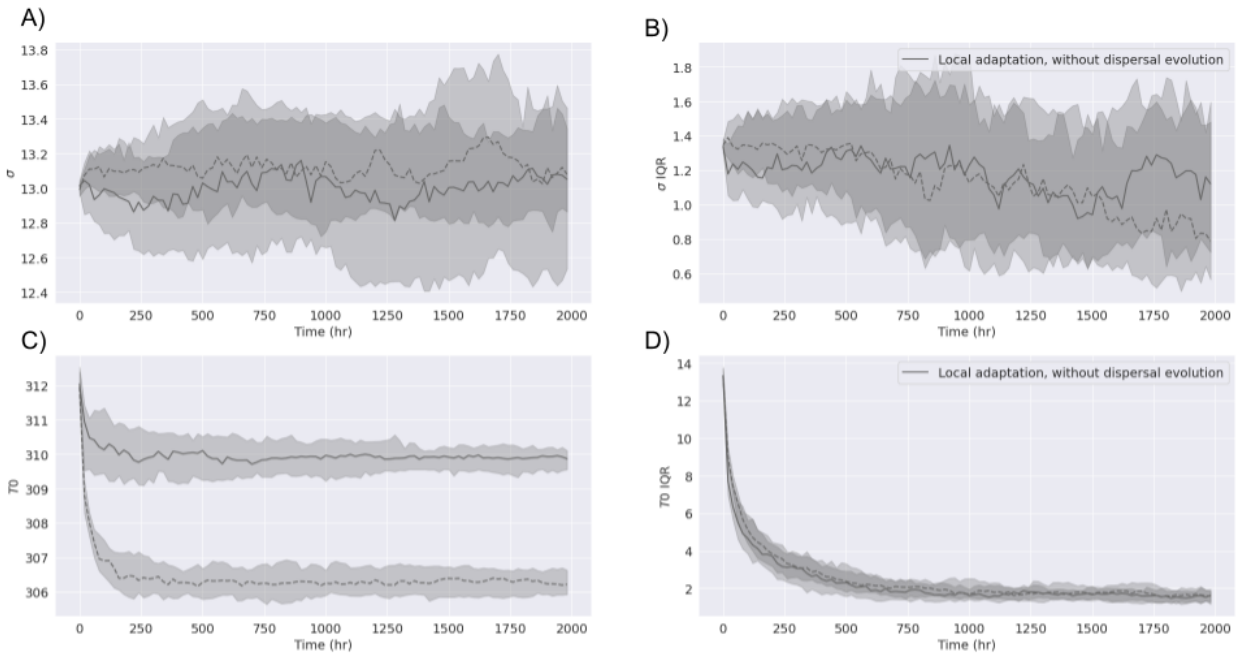


Figure 5.11: Comparison of average evolving trait value, its population level variation and among replicate variation. At every 20 hours simulation time, median and IQR of the evolving trait values of the 55th, 56th and 57th patch for the cold patch front and the 63th, 64th, 65th patch for the hot patch front are averaged, for simulations without dispersal evolution of the Gaussian curve model. Adapting parameters are $\sigma$: Standard deviation of the curve, $T_0$: Mean of curve; Panel A): Median of $\sigma$ trait with IQR for among replicates variation; Panel B): Median of patch population level IQR of $\sigma$ trait with IQR for among replicates; Panel C): Median of $T_0$ trait with IQR for among replicates variation; Panel D): Median of patch population level IQR of $T_0$ trait with IQR for among replicates.

## 5.2 R code for fitting

```
rm(list=ls())

# Data from the video analysis
library(ggplot2)
library(ggplot2)
library(reshape)
library(dplyr)
library(plyr)
library(ggpubr)
library(RColorBrewer)
library(rstan)
library(deSolve)
library(coda)
library(loo)
library(cowplot)
library(gridExtra)
library(ggmcmc)
library(nls.multstart)
library(rTPC)
library(tidyverse)


library(rethinking)
library(tidybayes)
library(tidybayes.rethinking)
library(cowplot)

library(rstan)
library(janitor)
library(patchwork)
library(brms)
library(tidybayes)



# load packages ------------------------------------------------------------
library(tidyverse)
library(rstan)
library(janitor)
library(patchwork)
library(brms)
library(tidybayes)

# options ------------------------------------------------------------------
## stan options
rstan_options(auto_write = TRUE)
options(mc.cores = parallel::detectCores())


#
# ##############################################################################################
# #r_tref * exp(e/k * (1/tref - 1/tK))*1/(1 + exp(eh/k * (1/(th + 273.15) - 1/tK)))
```

```
# #4 parameter model
d<-read.csv(file="~/Desktop/dATA FOR sAISMIT/growth_model_data_sum.csv" ,header= TRUE)
d=d%>% filter(d$speciesMT=='Tet_I')
d=d%>% filter(d$selection_temperature=='20')
d$log_r0_mean=log(d$r0_mean)
d$tK=d$temperature+273.15
d$tref=293.15
d$k=8.62e-5
d$log_r0_sd=log(d$r0_sd)

rep_name="c"
data_subset <- d[which(d$replicate==rep_name),]

nlform <-bf(log_r0_mean ~ log((rtref *exp(Hdd/k * (1/tref - 1/tK))*(1 + exp(-dGr/(k*tref)
    rtref ~ 1,
    Hdd~1,
    dGr ~ 1,
    dSr~1,
    #tref~1,
    dtref~1,
    dHdd~1,

    nl = TRUE)

nlprior <- c(prior(normal(0.2,0.05), nlpar = "rtref",lb=0,ub=1),
       prior(normal(0.75,0.05), nlpar = "Hdd",lb=0,ub=1),
       prior(normal(0.087,0.005), nlpar = "dGr",lb=0),
       prior(normal(0.0047,0.005), nlpar = "dSr",lb=0,ub=0.1),
       #prior(normal(293,10), nlpar = "tref",lb=0),
       prior(normal(0.02,0.005), nlpar = "dtref",lb=0),
       prior(normal(0.3,0.05), nlpar = "dHdd",lb=0)
)



mod_prot <- brm(formula = nlform,

          data = data_subset,

          prior = nlprior,
          control = list(adapt_delta = 0.999,max_treedepth=15),
          family = gaussian(),
          chains = 4,
          init = c(0.2,0.75,0.087,0.005,0.01,0.3),init_r=15,
          iter = 10000
)


print(summary(mod_prot))
pdf("~/Desktop/dATA FOR sAISMIT/Proteome/chain_plot.pdf")
pdf(paste("~/Desktop/dATA FOR sAISMIT/replicate_",rep_name,"/Proteome/chain_plot.pdf",sep
plot(mod_prot)
dev.off()
#
pairs_plot<-pairs(mod_prot)
ggsave(plot = pairs_plot,
```

```
   filename = paste0("~/Desktop/dATA FOR sAISMIT/Proteome/pairs_plot.png"),
   width = 15,
   height = 6)
ggsave(plot = pairs_plot,
   filename = paste("~/Desktop/dATA FOR sAISMIT/replicate_",rep_name,"/Proteome/pairs_plo
   width = 15,
   height = 6)

# Closing the graphical device
dev.off()
#
stancode(mod_prot)

prior_dist <-

(rnorm(1:80000,(0.2),0.05)) %>%
bind_cols() %>%
dplyr::rename("b_rtref_Intercept" = "...1") %>%
bind_cols()


prior_dist <-
(rnorm(1:80000,(0.75), 0.05)) %>%
bind_cols() %>%
dplyr::rename("b_Hdd_Intercept" = "...1") %>%
bind_cols(prior_dist)

prior_dist <-
(rnorm(1:80000,0.087, 0.005)) %>%
bind_cols() %>%
dplyr:: rename("b_dGr_Intercept" = "...1") %>%
bind_cols(prior_dist)

prior_dist <-
rnorm(1:80000,0.005,0.0005) %>%
bind_cols() %>%
# filter(...1 > 25) %>%
dplyr:: rename("b_dSr_Intercept" = "...1") %>%
bind_cols(prior_dist)
prior_dist <-
rnorm(1:80000,0.02,0.005) %>%
bind_cols() %>%
# filter(...1 > 25) %>%
dplyr:: rename("b_dtref_Intercept" = "...1") %>%
bind_cols(prior_dist)
prior_dist <-
rnorm(1:80000,0.3,0.05) %>%
bind_cols() %>%
# filter(...1 > 25) %>%
dplyr:: rename("b_dHdd_Intercept" = "...1") %>%
bind_cols(prior_dist) %>%

gather(., 'param', 'estimate', 1:ncol(.)) %>%
mutate(type = "prior")

dists <- mod_prot %>%
```

```
spread_draws(‘b_.*‘, regex = TRUE) %>%
gather(., ’param’, ’estimate’, 4:ncol(.)) %>%
mutate(type = "post") %>%
bind_rows(prior_dist)

plot_grid<-ggplot(dists, aes(x = estimate)) +
facet_wrap(~param, scales = "free") +
geom_density(aes(colour = type))

print(plot_grid)

ggsave(plot = plot_grid,
   filename = paste0("~/Desktop/dATA FOR sAISMIT/Proteome/post_curves.png"),
   width = 15,
   height = 6)
ggsave(plot = plot_grid,
   filename = paste("~/Desktop/dATA FOR sAISMIT/replicate_",rep_name,"/Proteome/post_curv
   width = 15,
   height = 6)
params <- mod_prot %>%
spread_draws(‘b_.*‘, regex = TRUE) %>%
gather(., ’param’, ’estimate’, 4:ncol(.)) %>%
separate(., param, c(’blah’, ’term’, ’blah2’), sep = ’_’) %>%
select(., -starts_with(’blah’)) %>%
filter(., !is.nan(estimate)) %>%
group_by(., term) %>%
mean_qi()

write.csv(params,
      file =paste0("~/Desktop/dATA FOR sAISMIT/Proteome/model_posteriors_parameters.csv")
      append = TRUE)

write.csv(params,
      file = paste("~/Desktop/dATA FOR sAISMIT/replicate_",rep_name,"/Proteome/model_post
      append = TRUE)
preds_prot <- data.frame(tK = seq(5+ 273.15, 40 + 273.15, length.out = 200),
                tref = 20 + 273.15,
                k = 8.62e-05,
                log_r0_sd = 1) %>%
add_fitted_draws(mod_prot ,re_formula = NA) %>%
data.frame() %>%
group_by(tK) %>%
mean_qi(estimate = .value)
#
preds_prot$estimate<-exp(preds_prot$estimate)
preds_prot$.upper<-exp(preds_prot$.upper)
preds_prot$.lower<-exp(preds_prot$.lower)

write.csv(preds_prot,
      file =paste0("~/Desktop/dATA FOR sAISMIT/Proteome/model_predictions.csv"),
      append = TRUE)

write.csv(preds_prot,
      file =paste("~/Desktop/dATA FOR sAISMIT/replicate_",rep_name,"/Proteome/model_predi
      append = TRUE)
Niche_plot_prot <-ggplot(preds_prot, aes(x = tK-273.15, y = estimate)) +
```

```
geom_line(color='coral1') +
geom_ribbon(aes(ymin = .lower, ymax = .upper), alpha = 0.2,fill='coral1') +
geom_pointrange(data = data_subset, aes(x = temperature, y = r0_mean, ymin =r0_mean-r0_sd

ggsave(plot = Niche_plot_prot,
   filename = paste0("~/Desktop/dATA FOR sAISMIT/Proteome/fit_model.png"),
   width = 15,
   height = 6)


ggsave(plot = Niche_plot_prot,
   filename =paste("~/Desktop/dATA FOR sAISMIT/replicate_",rep_name,"/Proteome/fit_model.
   width = 15,
   height = 6)

ggsave(plot = Niche_plot_prot,
   filename = paste0("~/Desktop/dATA FOR sAISMIT/fit_model.png"),
   width = 15,
   height = 6)

##MMRT
################################################################
nlform <-bf(log_r0_mean ~ log((rtref *tK*(1/tref)*exp((Hdd-DCp*(tref-tm))/(k *tref))*exp(
  rtref ~ 1,
  Hdd ~ 1,
  DCp~1,
  dtref~1,
  dHdd~1,
  tm~1,
  nl = TRUE)


nlprior <- c(prior(normal(0.2,0.2), nlpar = "rtref",lb=0.01,ub=0.5),
 prior(normal(0.1,0.05), nlpar = "Hdd",lb=0,ub=0.5),
 prior(normal(0.06,0.025), nlpar = "DCp",lb=0.01),
 #   prior(normal(0.0047,0.001), nlpar = "dSr",lb=0),
 prior(normal(0.05,0.005), nlpar = "dtref",lb=0.01,ub=0.1),
 prior(normal(0.5,0.05), nlpar = "dHdd",lb=0),
 prior(normal(310,10), nlpar = "tm",lb=270)

)

mod_mmrt <- brm(formula = nlform,
      data = data_subset,

      prior = nlprior,
      control = list(adapt_delta = 0.999,max_treedepth=15),
      family = gaussian(),
      chains = 4,
      init = c(0.2,0.5,0.06,0.05,0.3,310),init_r=15,
      iter = 10000
)


print(summary(mod_mmrt))
pdf("~/Desktop/dATA FOR sAISMIT/MMRT/chain_plot.pdf")
```

```
pdf( paste("~/Desktop/dATA FOR sAISMIT/replicate_",rep_name,"/MMRT/chain_plot.pdf",sep="")
plot(mod_mmrt)
dev.off()

pairs_plot<-pairs(mod_mmrt)
ggsave(plot = pairs_plot,
   filename = paste0("~/Desktop/dATA FOR sAISMIT/MMRT/pairs_plot.png"),
   width = 15,
   height = 6)
ggsave(plot = pairs_plot,
   filename = paste("~/Desktop/dATA FOR sAISMIT/replicate_",rep_name,"/MMRT/pairs_plot.png
   width = 15,
   height = 6)
# Customizing the output
#pdf(paste0("~/Desktop/dATA FOR sAISMIT/Proteome/", file_name, "_pairs_plot.pdf"))# Paper

# Creating a plot
#plot(fit_test_mod_2)

# Closing the graphical device
dev.off()

stancode(mod_mmrt)

prior_dist <-

(rnorm(1:80000,(0.2),0.2)) %>%
bind_cols() %>%
dplyr::rename("b_rtref_Intercept" = "...1") %>%
bind_cols()

prior_dist <-
(rnorm(1:80000,(0.1), 0.05)) %>%
bind_cols() %>%
dplyr::rename("b_Hdd_Intercept" = "...1") %>%
bind_cols(prior_dist)

prior_dist <-
(rnorm(1:80000,0.06, 0.025)) %>%
bind_cols() %>%
dplyr:: rename("b_DCp_Intercept" = "...1") %>%
bind_cols(prior_dist)

prior_dist <-
rnorm(1:80000,0.05,0.005) %>%
bind_cols() %>%
# filter(...1 > 25) %>%
dplyr:: rename("b_dtref_Intercept" = "...1") %>%
bind_cols(prior_dist)
prior_dist <-
rnorm(1:80000,0.5,0.05) %>%
bind_cols() %>%
# filter(...1 > 25) %>%
dplyr:: rename("b_dHdd_Intercept" = "...1") %>%
bind_cols(prior_dist)
prior_dist <-
```

```
rnorm(1:80000,310,10) %>%
bind_cols() %>%
# filter(...1 > 25) %>%
dplyr:: rename("b_tm_Intercept" = "...1") %>%
bind_cols(prior_dist) %>%

gather(., 'param', 'estimate', 1:ncol(.)) %>%
mutate(type = "prior")
bind_rows(prior_dist)

dists <- mod_mmrt %>%
spread_draws(`b_.*`, regex = TRUE) %>%
gather(., 'param', 'estimate', 4:ncol(.)) %>%
mutate(type = "post") %>%
bind_rows(prior_dist)

plot_grid<-ggplot(dists, aes(x = estimate)) +
facet_wrap(~param, scales = "free") +
geom_density(aes(colour = type))

print(plot_grid)

ggsave(plot = plot_grid,
   filename = paste0("~/Desktop/dATA FOR sAISMIT/MMRT/post_curves.png"),
   width = 15,
   height = 6)
ggsave(plot = plot_grid,
   filename = paste("~/Desktop/dATA FOR sAISMIT/replicate_",rep_name,"/MMRT/post_curves.pn
   width = 15,
   height = 6)
params <- mod_mmrt %>%
spread_draws(`b_.*`, regex = TRUE) %>%
gather(., 'param', 'estimate', 4:ncol(.)) %>%
separate(., param, c('blah', 'term', 'blah2'), sep = '_') %>%
select(., -starts_with('blah')) %>%
filter(., !is.nan(estimate)) %>%
group_by(., term) %>%
mean_qi()

write.csv(params,
      file =paste0("~/Desktop/dATA FOR sAISMIT/MMRT/model_posteriors_parameters.csv"),
      append = TRUE)
write.csv(params,
      file =paste("~/Desktop/dATA FOR sAISMIT/replicate_",rep_name,"/MMRT/model_posteriors
      )

preds_mmrt <- data.frame(tK = seq(5+ 273.15, 40 + 273.15, length.out = 200),
                tref = 20 + 273.15,
                k = 8.62e-05,
                log_r0_sd = 1) %>%
add_fitted_draws(mod_mmrt ,re_formula = NA) %>%
data.frame() %>%
group_by(tK) %>%
mean_qi(estimate = .value)
#
preds_mmrt$estimate<-exp(preds_mmrt$estimate)
```

```
preds_mmrt$.upper<-exp(preds_mmrt$.upper)
preds_mmrt$.lower<-exp(preds_mmrt$.lower)

write.csv(preds_mmrt,
      file =paste0("~/Desktop/dATA FOR sAISMIT/MMRT/model_predictions.csv"),
      append = TRUE)
write.csv(preds_mmrt,
      file =paste("~/Desktop/dATA FOR sAISMIT/replicate_",rep_name,"/MMRT/model_predictio
      append = TRUE)


Niche_plot_mrt <-ggplot(preds_mmrt, aes(x = tK-273.15, y = estimate)) +
geom_line(color='darkgoldenrod1') +
geom_ribbon(aes(ymin = .lower, ymax = .upper), alpha = 0.2,fill='darkgoldenrod1') +
geom_pointrange(data = data_subset, aes(x = temperature, y = r0_mean, ymin =r0_mean-r0_sd


#p<-p+
#  geom_line(color='darkgoldenrod1') +
#  geom_ribbon(aes(ymin = .lower, ymax = .upper), alpha = 0.2,fill='darkgoldenrod1')

ggsave(plot = Niche_plot_mrt,
   filename = paste0("~/Desktop/dATA FOR sAISMIT/MMRT/fit_model.png"),
   width = 15,
   height = 6)

ggsave(plot = Niche_plot_mrt,
   filename =paste("~/Desktop/dATA FOR sAISMIT/replicate_",rep_name,"/MMRT/fit_model.png"
   width = 15,
   height = 6)

ggsave(plot =Niche_plot_mrt,
   filename = paste0("~/Desktop/dATA FOR sAISMIT/fit_model.png"),
   width = 15,
   height = 6)



#EAAR
########################
nlform <-bf(log_r0_mean ~ log((rtref*exp((Eb-(Edh*(1-tref/tm)+Edcp*(tref-tm-tref*log(tref/
            rtref ~ 1,
            Eb ~ 1,
            Edcp~1,
            Edh~1,
            dtref~1,
            dHdd~1,
            tm~1,
            nl = TRUE)


nlprior <- c(prior(normal(0.2,0.05), nlpar = "rtref",lb=0.01,ub=1),
             prior(normal(0.1,0.05), nlpar = "Eb",lb=0.0, ub=1.2),
             prior(normal(0.1,0.05), nlpar = "Edh",lb=0.0),
             prior(normal(0.1,0.05), nlpar = "Edcp",lb=0.0),
             #   prior(normal(0.0047,0.001), nlpar = "dSr",lb=0),
```

```
              prior(normal(0.01,0.005), nlpar = "dtref",lb=0.001),
              prior(normal(0.5,0.25), nlpar = "dHdd",lb=0.01,ub=1.2),
              prior(normal(310,10), nlpar = "tm",lb=300)

)

mod_eaar <- brm(formula = nlform,
                data = data_subset,

                prior = nlprior,
                control = list(adapt_delta = 0.999,max_treedepth=15),
                family = gaussian(),
                chains = 4,
                init = c(0.2,0.1,0.5,0.05,0.01,0.3,310),init_r=15,
                iter = 10000
)


print(summary(mod_eaar))
pdf("~/Desktop/dATA FOR sAISMIT/EAAR/chain_plot.pdf")
pdf(paste("~/Desktop/dATA FOR sAISMIT/replicate_",rep_name,"/EAAR/chain_plot.pdf",sep="")
plot(mod_eaar)
dev.off()
dev.off()
pairs_plot<-pairs(mod_eaar)
ggsave(plot = pairs_plot,
       filename = paste0("~/Desktop/dATA FOR sAISMIT/EAAR/pairs_plot.png"),
       width = 15,
       height = 6)

ggsave(plot = pairs_plot,
       filename = paste("~/Desktop/dATA FOR sAISMIT/replicate_",rep_name,"/EAAR/pairs_plo
       width = 15,
       height = 6)
# Closing the graphical device
dev.off()

stancode(mod_eaar)


prior_dist <-

  (rnorm(1:80000,(0.2),0.05)) %>%
  bind_cols() %>%
  dplyr::rename("b_rtref_Intercept" = "...1") %>%
  bind_cols()


prior_dist <-
  (rnorm(1:80000,(0.5), 0.05)) %>%
  bind_cols() %>%
  dplyr::rename("b_Eb_Intercept" = "...1") %>%
  bind_cols(prior_dist)

prior_dist <-
  (rnorm(1:80000,1, 0.05)) %>%
```

```
  bind_cols() %>%
  dplyr:: rename("b_Edh_Intercept" = "...1") %>%
  bind_cols(prior_dist)

prior_dist <-
  rnorm(1:80000,1,0.05) %>%
  bind_cols() %>%
  # filter(...1 > 25) %>%
  dplyr:: rename("b_Edcp_Intercept" = "...1") %>%
  bind_cols(prior_dist)
prior_dist <-
  rnorm(1:80000,0.5,0.25) %>%
  bind_cols() %>%
  # filter(...1 > 25) %>%
  dplyr:: rename("b_dHdd_Intercept" = "...1") %>%
  bind_cols(prior_dist)
prior_dist <-
  rnorm(1:80000,0.01,0.005) %>%
  bind_cols() %>%
  # filter(...1 > 25) %>%
  dplyr:: rename("b_dtref_Intercept" = "...1") %>%
  bind_cols(prior_dist)
prior_dist <-
  rnorm(1:80000,310,10) %>%
  bind_cols() %>%
  # filter(...1 > 25) %>%
  dplyr:: rename("b_tm_Intercept" = "...1") %>%
  bind_cols(prior_dist) %>%

  gather(., 'param', 'estimate', 1:ncol(.)) %>%
  mutate(type = "prior")
dists <- mod_eaar %>%
  spread_draws(`b_.*`, regex = TRUE) %>%
  gather(., 'param', 'estimate', 4:ncol(.)) %>%
  mutate(type = "post") %>%
  bind_rows(prior_dist)

dists <- mod_eaar %>%
  spread_draws(`b_.*`, regex = TRUE) %>%
  gather(., 'param', 'estimate', 4:ncol(.)) %>%
  mutate(type = "post") %>%
  bind_rows(prior_dist)

plot_grid<-ggplot(dists, aes(x = estimate)) +
  facet_wrap(~param, scales = "free") +
  geom_density(aes(colour = type))

print(plot_grid)

ggsave(plot = plot_grid,
       filename = paste0("~/Desktop/dATA FOR sAISMIT/EAAR/post_curves.png"),
       width = 15,
       height = 6)
ggsave(plot = plot_grid,
       filename = paste("~/Desktop/dATA FOR sAISMIT/replicate_",rep_name,"/EAAR/post_curv
       width = 15,
```

```
       height = 6)
params <- mod_eaar %>%
  spread_draws(`b_.*`, regex = TRUE) %>%
  gather(., 'param', 'estimate', 4:ncol(.)) %>%
  separate(., param, c('blah', 'term', 'blah2'), sep = '_') %>%
  select(., -starts_with('blah')) %>%
  filter(., !is.nan(estimate)) %>%
  group_by(., term) %>%
  mean_qi()

write.csv(params,
          file =paste0("~/Desktop/dATA FOR sAISMIT/EAAR/model_posteriors_parameters.csv")
          append = TRUE)
write.csv(params,
          file =paste("~/Desktop/dATA FOR sAISMIT/replicate_",rep_name,"/EAAR/model_poste
          append = TRUE)

preds_eaar <- data.frame(tK = seq(5+ 273.15, 40 + 273.15, length.out = 200),
                     tref = 20 + 273.15,
                     k = 8.62e-05,
                     log_r0_sd = 1) %>%
  add_fitted_draws(mod_eaar ,re_formula = NA) %>%
  data.frame() %>%
  group_by(tK) %>%
  mean_qi(estimate = .value)
#
preds_eaar$estimate<-exp(preds_eaar$estimate)
preds_eaar$.upper<-exp(preds_eaar$.upper)
preds_eaar$.lower<-exp(preds_eaar$.lower)

write.csv(preds_eaar,
          file =paste0("~/Desktop/dATA FOR sAISMIT/replicate_",rep_name,"/EAAR/model_pred
          append = TRUE)
write.csv(preds_eaar,
          file =paste0("~/Desktop/dATA FOR sAISMIT/EAAR/model_predictions.csv"),
          append = TRUE)
Niche_plot_eaar <-ggplot(preds_eaar, aes(x = tK-273.15, y = estimate)) +
  geom_line(color='aquamarine3') +
  geom_ribbon(aes(ymin = .lower, ymax = .upper), alpha = 0.2,fill='aquamarine3') +
  geom_pointrange(data = data_subset, aes(x = temperature, y = r0_mean, ymin =r0_mean-r0_


ggsave(plot = Niche_plot_eaar,
       filename = paste0("~/Desktop/dATA FOR sAISMIT/EAAR/fit_model.png"),
       width = 15,
       height = 6)
ggsave(plot = Niche_plot_eaar,
       filename = paste0("~/Desktop/dATA FOR sAISMIT/replicate_",rep_name,"/EAAR/fit_model
       width = 15,
       height = 6)

ggsave(plot =  Niche_plot_eaar,
       filename = paste0("~/Desktop/dATA FOR sAISMIT/fit_model.png"),
       width = 15,
       height = 6)
```

```
p<-ggplot(data=preds_eaar, mapping=aes(x = tK-273.15, y = estimate)) + geom_line(color='c
    geom_ribbon(data=preds_eaar,mapping=aes(ymin = .lower, ymax = .upper), alpha = 0.2,fi
    geom_ribbon(data=preds_prot,mapping=aes(ymin = .lower, ymax = .upper), alpha = 0.2,fi
    geom_ribbon(data=preds_mmrt,mapping=aes(ymin = .lower, ymax = .upper), alpha = 0.2,fi
    theme(legend.position = "left")

ggsave(plot = p,
         filename = paste0("~/Desktop/dATA FOR sAISMIT/fit_model.png"),
         width = 15,
         height = 6)
##weights

waic1 <- waic(mod_eaar)
write.csv(waic1$estimates,paste("replicate_",rep_name,"/EAAR/waic.csv",sep=""))
waic2 <- waic(mod_prot)
write.csv(waic2$estimates,paste("replicate_",rep_name,"/Proteome/waic.csv",sep=""))
waic3 <- waic(mod_mmrt)
write.csv(waic3$estimates,paste("replicate_",rep_name,"/MMRT/waic.csv",sep=""))
waics <- c(
waic1$estimates["elpd_waic", 1],
waic2$estimates["elpd_waic", 1],
waic3$estimates["elpd_waic", 1])

loo1 <- loo(mod_eaar)
write.csv(loo1$estimates,paste("replicate_",rep_name,"/EAAR/loo.csv",sep=""))
loo2 <- loo(mod_prot)
write.csv(loo2$estimates,paste("replicate_",rep_name,"/Proteome/loo.csv",sep=""))
loo3 <- loo(mod_mmrt)
write.csv(loo3$estimates,paste("replicate_",rep_name,"/MMRT/loo.csv",sep=""))
lpd_point <- cbind(
loo1$pointwise[,"elpd_loo"],
loo2$pointwise[,"elpd_loo"],
loo3$pointwise[,"elpd_loo"])

waic_wts <- exp(waics) / sum(exp(waics))
pbma_wts <- pseudobma_weights(lpd_point, BB=FALSE)
pbma_BB_wts <- pseudobma_weights(lpd_point) # default is BB=TRUE
stacking_wts <- stacking_weights(lpd_point)
round(cbind(waic_wts, pbma_wts, pbma_BB_wts, stacking_wts), 2)
write.csv(round(cbind(waic_wts, pbma_wts, pbma_BB_wts, stacking_wts), 2),paste("replicate
write.csv(data_subset,paste("replicate_",rep_name,"/data.csv",sep=""))
```

# Bibliography


[1] G. E. Allen and C. Dytham. An efficient method for stochastic simulation of biological populations in continuous time. *Biosystems*, 98(1):37–42, Oct. 2009. ISSN 0303-2647. doi: 10.1016/j.biosystems.2009.07.003. URL https://www.sciencedirect.com/science/article/pii/S0303264709001130.

[2] C. J. Alster, P. Baas, M. D. Wallenstein, N. G. Johnson, and J. C. von Fischer. Temperature sensitivity as a microbial trait using parameters from macromolecular rate theory. *Frontiers in Microbiology*, 7, 2016. ISSN 1664-302X. doi: 10.3389/fmicb.2016.01821. URL https://www.frontiersin.org/article/10.3389/fmicb.2016.01821.

[3] P. Amarasekare. Effects of climate warming on consumer-resource interactions: a latitudinal perspective. *Frontiers in Ecology and Evolution*, 7:146, 2019.

[4] M. Andrade-Restrepo, N. Champagnat, and R. Ferrière. Local adaptation, dispersal evolution, and the spatial eco-evolutionary dynamics of invasion. *Ecology letters*, 22 (5):767–777, 2019.

[5] M. J. Angilletta, P. H. Niewiarowski, and C. A. Navas. The evolution of thermal physiology in ectotherms. *Journal of Thermal Biology*, 27(4):249–268, 2002. ISSN 0306-4565. doi: https://doi.org/10.1016/S0306-4565(01)00094-8. URL https://www.sciencedirect.com/science/article/pii/S0306456501000948.

[6] M. B. Araújo, F. Ferri-Yáñez, F. Bozinovic, P. A. Marquet, F. Valladares, and S. L. Chown. Heat freezes niche evolution. *Ecology Letters*, 16(9):1206–1219, 2013. doi: https://doi.org/10.1111/ele.12155. URL https://onlinelibrary.wiley.com/doi/abs/10.1111/ele.12155.

[7] J. I. Arroyo, B. Díez, C. P. Kempes, G. B. West, and P. A. Marquet. A general theory for temperature dependence in biology. *Proceedings of the National Academy of Sciences*, 119(30):e2119872119, 2022. doi: 10.1073/pnas.2119872119. URL https://www.pnas.org/doi/abs/10.1073/pnas.2119872119.

[8] S. Bathiany, V. Dakos, M. Scheffer, and T. M. Lenton. Climate models predict increasing temperature variability in poor countries. *Science Advances*, 4(5):eaar5809, 2018. doi: 10.1126/sciadv.aar5809. URL https://www.science.org/doi/abs/10.1126/sciadv.aar5809.

[9] A. F. Bennett and R. E. Lenski. Evolutionary adaptation to temperature ii. thermal niches of experimental lines of escherichia coli. *Evolution*, 47(1):1–12, 1993. doi: https://doi.org/10.1111/j.1558-5646.1993.tb01194.x. URL https://onlinelibrary.wiley.com/doi/abs/10.1111/j.1558-5646.1993.tb01194.x.

[10] D. Berger, E. Postma, W. U. Blanckenhorn, and R. J. Walters. Quantitative genetic divergence and standing genetic (co) variance in thermal reaction norms along latitude. *Evolution*, 67(8):2385–2399, 2013.

[11] R. J. H. Beverton and S. J. Holt. Introduction Theoretical Methods in the Study of Fishery Dynamics. In R. J. H. Beverton and S. J. Holt, editors, *On the Dynamics of Exploited Fish Populations*, Fish & Fisheries Series, pages 21–26. Springer Netherlands, Dordrecht, 1993. ISBN 9789401121064. doi: 10.1007/978-94-011-2106-4_1. URL https://doi.org/10.1007/978-94-011-2106-4_1.

[12] J. C. BISCHOF and X. HE. Thermal stability of proteins. *Annals of the New York Academy of Sciences*, 1066(1):12–33, 2006. doi: https://doi.org/10.1196/annals.1363.003. URL https://nyaspubs.onlinelibrary.wiley.com/doi/abs/10.1196/annals.1363.003.

[13] K. Bomblies and C. L. Peichel. Genetics of adaptation. *Proceedings of the National Academy of Sciences*, 119(30):e2122152119, 2022. doi: 10.1073/pnas.2122152119. URL https://www.pnas.org/doi/abs/10.1073/pnas.2122152119.

[14] M. Breen, C. Kemena, P. Vlasov, C. Notredame, and F. Kondrashov. Epistasis as the primary factor in molecular evolution. *Nature*, 490:535–8, 10 2012. doi: 10.1038/nature11510.

[15] J. Brown, J. Gillooly, A. Allen, V. Savage, and G. West. Toward a metabolic theory of ecology. *Ecology*, 85:1771–1789, 07 2004. doi: 10.1890/03-9000.

[16] L. B. Buckley and J. G. Kingsolver. Evolution of thermal sensitivity in changing and variable climates. *Annual Review of Ecology, Evolution, and Systematics*, 52:563–586, 2021.

[17] E. Butin, A. H. Porter, and J. Elkinton. Adaptation during biological invasions and the case of adelges tsugae. *Evolutionary Ecology Research*, 7(6):887–900, 2005.

[18] P.-C. Bürkner. brms: An R package for Bayesian multilevel models using Stan. *Journal of Statistical Software*, 80(1):1–28, 2017. doi: 10.18637/jss.v080.i01.

[19] J. A. Carbonell, Y.-J. Wang, and R. Stoks. Evolution of cold tolerance and thermal plasticity in life history, behaviour and physiology during a poleward range expansion. *Journal of Animal Ecology*, 90(7):1666–1677, 2021. doi: https://doi.org/10.1111/1365-2656.13482. URL https://besjournals.onlinelibrary.wiley.com/doi/abs/10.1111/1365-2656.13482.

[20] P. Chen and E. Shakhnovich. Thermal adaptation of viruses and bacteria. *Biophysical journal*, 98:1109–18, 04 2010. doi: 10.1016/j.bpj.2009.11.048,.

[21] A. Clarke. Costs and consequences of evolutionary temperature adaptation. *Trends in Ecology Evolution*, 18(11):573–581, 2003. ISSN 0169-5347. doi: https://doi.org/10.1016/j.tree.2003.08.007. URL https://www.sciencedirect.com/science/article/pii/S0169534703002544.

[22] R. I. Colautti and S. C. H. Barrett. Rapid adaptation to climate facilitates range expansion of an invasive plant. *Science*, 342(6156):364–366, 2013. doi: 10.1126/science.1242121. URL https://www.science.org/doi/abs/10.1126/science.1242121.

[23] R. Corkrey, J. Olley, D. Ratkowsky, T. McMeekin, and T. Ross. Universality of thermodynamic constants governing biological growth rates. *PLOS ONE*, 7(2):1–8, 02 2012. doi: 10.1371/journal.pone.0032003. URL https://doi.org/10.1371/journal.pone.0032003.

[24] R. Couñago, S. Chen, and Y. Shamoo. In vivo molecular evolution reveals biophysical origins of organismal fitness. *Molecular Cell*, 22(4):441–449, 2006. ISSN

1097-2765. doi: https://doi.org/10.1016/j.molcel.2006.04.012. URL https://www.sciencedirect.com/science/article/pii/S1097276506002607.

[25] A. Cruz, M. Hebly, G.-H. Duong, A. Wahl, J. Pronk, S. Heijnen, P. Daran-Lapujade, and W. Gulik. Similar temperature dependencies of glycolytic enzymes: An evolutionary adaptation to temperature dynamics? *BMC systems biology*, 6:151, 12 2012. doi: 10.1186/1752-0509-6-151.

[26] A. J. Cullum, A. F. Bennett, and R. E. Lenski. Evolutionary adaptation to temperature. ix. preadaptation to novel stressful environments of escherichia coli adapted to high temperature. *Evolution*, 55(11):2194–2202, 2001. ISSN 00143820, 15585646. URL http://www.jstor.org/stable/2680351.

[27] G. de Jong and A. Imasheva. Genetic variance in temperature dependent adult size deriving from physiological genetic variation at temperature boundaries. *Genetica*, 110 (2):195–207, 2000.

[28] P. A. del Giorgio and J. J. Cole. Bacterial growth efficiency in natural aquatic systems. *Annual Review of Ecology and Systematics*, 29(1):503–541, 1998. doi: 10.1146/annurev.ecolsys.29.1.503. URL https://doi.org/10.1146/annurev.ecolsys.29.1.503.

[29] A. I. Dell, S. Pawar, and V. M. Savage. Systematic variation in the temperature dependence of physiological and ecological traits. *PNAS*, 108(26):10591–10596, 2011. doi: 10.1073/pnas.1015178108. URL https://www.pnas.org/doi/abs/10.1073/pnas.1015178108.

[30] J. P. DeLong, J. P. Gibert, T. M. Luhring, G. Bachman, B. Reed, A. Neyer, and K. L. Montooth. The combined effects of reactant kinetics and enzyme stability explain the temperature dependence of metabolic rates. *Ecology and Evolution*, 7(11):3940–3950, 2017. doi: https://doi.org/10.1002/ece3.2955. URL https://onlinelibrary.wiley.com/doi/abs/10.1002/ece3.2955.

[31] R. B. Ehnes, B. C. Rall, and U. Brose. Phylogenetic grouping, curvature and metabolic scaling in terrestrial invertebrates. *Ecology Letters*, 14(10):993–1000, 2011. doi: https://doi.org/10.1111/j.1461-0248.2011.01660.x. URL https://onlinelibrary.wiley.com/doi/abs/10.1111/j.1461-0248.2011.01660.x.

[32] H. Eyring. The activated complex and the absolute rate of chemical reactions. *Chemical Reviews*, 17(1):65–77, 1935. doi: 10.1021/cr60056a006. URL https://doi.org/10.1021/cr60056a006.

[33] G. Feller. Protein stability and enzyme activity at extreme biological temperatures. *Journal of Physics: Condensed Matter*, 22(32):323101, jul 2010. doi: 10.1088/0953-8984/22/32/323101. URL https://doi.org/10.1088/0953-8984/22/32/323101.

[34] G. Feller and C. Gerday. Psychrophilic enzymes: Hot topics in cold adaptation. *Nature reviews. Microbiology*, 1:200–8, 01 2004. doi: 10.1038/nrmicro773.

[35] P. A. Fields and G. N. Somero. Hot spots in cold adaptation: Localized increases in conformational flexibility in lactate dehydrogenase a¡sub¿4¡/sub¿ orthologs of antarctic notothenioid fishes. *Proceedings of the National Academy of Sciences*, 95(19):11476–11481, 1998. doi: 10.1073/pnas.95.19.11476. URL https://www.pnas.org/doi/abs/10.1073/pnas.95.19.11476.

[36] P. A. Fields, Y. Dong, X. Meng, G. N. Somero, J. E. Podrabsky, J. H. Stillman, and L. Tomanek. Adaptations of protein structure and function to temperature: there is more than one way to 'skin a cat'. *Journal of Experimental Biology*, 218(12):1801–1811, 06 2015. ISSN 0022-0949. doi: 10.1242/jeb.114298. URL https://doi.org/10.1242/jeb.114298.

[37] J. M. Fox, M. Zhao, M. J. Fink, K. Kang, and G. M. Whitesides. The molecular origin of enthalpy/entropy compensation in biomolecular recognition. *Annual Review of Biophysics*, 47(1):223–250, 2018. doi: 10.1146/annurev-biophys-070816-033743. URL https://doi.org/10.1146/annurev-biophys-070816-033743. PMID: 29505727.

[38] A. G. Fraser, R. S. Kamath, P. Zipperlen, M. Martinez-Campos, M. Sohrmann, and J. Ahringer. Functional genomic analysis of c. elegans chromosome i by systematic rna interference. *Nature*, 408(6810):325–330, 2000.

[39] M. Frazier, R. B. Huey, and D. Berrigan. Thermodynamics constrains the evolution of insect population growth rates:"warmer is better". *The American Naturalist*, 168(4):512–520, 2006.

[40] E. Fronhofer and F. Altermatt. Eco-evolutionary feedbacks during experimental range expansions. *Nature Communications*, 6:6844, 04 2015. doi: 10.1038/ncomms7844.

[41] E. A. Fronhofer, L. Govaert, M. I. O'Connor, S. J. Schreiber, and F. Altermatt. The shape of density dependence and the relationship between population growth, intraspecific competition and equilibrium population density. *bioRxiv*, 2020. doi: 10.1101/485946. URL https://www.biorxiv.org/content/early/2020/06/02/485946.

[42] G. W. Gilchrist and R. B. Huey. Plastic and Genetic Variation in Wing Loading as a Function of Temperature Within and Among Parallel Clines in Drosophila subobscura1. *Integrative and Comparative Biology*, 44(6):461–470, 12 2004. ISSN 1540-7063. doi: 10.1093/icb/44.6.461. URL https://doi.org/10.1093/icb/44.6.461.

[43] D. T. Gillespie et al. Stochastic simulation of chemical kinetics. *Annual review of physical chemistry*, 58(1):35–55, 2007.

[44] J. F. Gillooly, J. H. Brown, G. B. West, V. M. Savage, and E. L. Charnov. Effects of size and temperature on metabolic rate. *Science*, 293(5538):2248–2251, 2001. doi: 10.1126/science.1061967. URL https://www.science.org/doi/abs/10.1126/science.1061967.

[45] G. M. Grimaud. *Modelling the temperature effect on phytoplankton: from acclimation to adaptation*. PhD thesis, 06 2016.

[46] I. Hanski, C. Erälahti, M. Kankare, O. Ovaskainen, and H. Sirén. Variation in migration propensity among individuals maintained by landscape structure. *Ecol. Lett.*, 7(10):958–966, 2004. doi: https://doi.org/10.1111/j.1461-0248.2004.00654.x. URL https://onlinelibrary.wiley.com/doi/abs/10.1111/j.1461-0248.2004.00654.x.

[47] M. Harms and J. Thornton. Evolutionary biochemistry: Revealing the historical and physical causes of protein properties. *Nature reviews. Genetics*, 14:559–71, 08 2013. doi: 10.1038/nrg3540.

[48] K. M. Hart, M. J. Harms, B. H. Schmidt, C. Elya, J. W. Thornton, and S. Marqusee. Thermodynamic system drift in protein evolution. *PLOS Biology*, 12(11):1–12, 11 2014. doi: 10.1371/journal.pbio.1001994. URL https://doi.org/10.1371/journal.pbio.1001994.

[49] R. Hickling, D. Roy, J. Hill, and C. Thomas. A northward shift of range margins in british odonata. *Global Change Biology*, 11:502 – 506, 01 2005. doi: 10.1111/j.1365-2486.2005.00904.x.

[50] C. N. Hinshelwood. *The chemical kinetics of the bacterial cell,*. The Clarendon Press, Oxford, 1946. OCLC: 2366642.

[51] J. Hobbs, W. Jiao, A. Easter, E. Parker, L. Schipper, and V. Arcus. Change in heat capacity for enzyme catalysis determines temperature dependence of enzyme catalyzed rates. *ACS chemical biology*, 12, 02 2017. doi: 10.1021/acschembio.7b00065.

[52] P. W. Hochachka and G. N. Somero. *Biochemical adaptation: mechanism and process in physiological evolution*. Oxford university press, 2002.

[53] R. Holt. On the evolutionary ecology of species' ranges. *Evolutionary Ecology Research*, 5:159–178, 02 2003.

[54] R. B. Huey, G. W. Gilchrist, M. L. Carlson, D. Berrigan, and L. Serra. Rapid evolution of a geographic cline in size in an introduced fly. *Science*, 287(5451):308–309, 2000. doi: 10.1126/science.287.5451.308. URL https://www.science.org/doi/abs/10.1126/science.287.5451.308.

[55] L. T. Jensen, F. E. Cockerell, T. N. Kristensen, L. Rako, V. Loeschcke, S. W. McKechnie, and A. A. Hoffmann. Adult heat tolerance variation in drosophila melanogaster is not related to hsp70 expression. *Journal of Experimental Zoology Part A: Ecological Genetics and Physiology*, 313A(1):35–44, 2010. doi: https://doi.org/10.1002/jez.573. URL https://onlinelibrary.wiley.com/doi/abs/10.1002/jez.573.

[56] F. H. Johnson and I. Lewin. The growth rate of e. coli in relation to temperature, quinine and coenzyme. *Journal of Cellular and Comparative Physiology*, 28(1):47–75, 1946. doi: https://doi.org/10.1002/jcp.1030280104. URL https://onlinelibrary.wiley.com/doi/abs/10.1002/jcp.1030280104.

[57] I. Karl, T. Schmitt, and K. Fischer. Phosphoglucose isomerase genotype affects life-history traits and cold stress resistance in a copper butterfly. *Functional Ecology*, 22(5):887–894, 2008. doi: https://doi.org/10.1111/j.1365-2435.2008.01438.x. URL https://besjournals.onlinelibrary.wiley.com/doi/abs/10.1111/j.1365-2435.2008.01438.x.

[58] S. Karve, P. Dasmeh, J. Zheng, and A. Wagner. Low protein expression enhances phenotypic evolvability by intensifying selection on folding stability. *Nature ecology & evolution*, 2022.

[59] M. Kelly. Adaptation to climate change through genetic accommodation and assimilation of plastic phenotypes. *Philosophical Transactions of the Royal Society B: Biological Sciences*, 374(1768):20180176, 2019. doi: 10.1098/rstb.2018.0176. URL https://royalsocietypublishing.org/doi/abs/10.1098/rstb.2018.0176.

[60] J. Knies, J. Kingsolver, and C. Burch. Hotter is better and broader: Thermal sensitivity of fitness in a population of bacteriophages. *The American Naturalist*, 173(4):419–430, 2009. doi: 10.1086/597224. URL https://doi.org/10.1086/597224. PMID: 19232002.

[61] R. L. Kordas, C. D. Harley, and M. I. O'Connor. Community ecology in a warming world: The influence of temperature on interspecific interactions in marine systems. *Journal of Experimental Marine Biology and Ecology*, 400(1):218–226, 2011. ISSN 0022-0981. doi: https://doi.org/10.1016/j.jembe.2011.02.029. URL https://www.sciencedirect.com/science/article/pii/S0022098111000773. Global change in marine ecosystems.

[62] L. T. Lancaster, R. Y. Dudaniec, B. Hansson, and E. I. Svensson. Latitudinal shift in thermal niche breadth results from thermal release during a climate-mediated range expansion. *Journal of Biogeography*, 42(10):1953–1963, 2015. doi: https://doi.org/10.1111/jbi.12553. URL https://onlinelibrary.wiley.com/doi/abs/10.1111/jbi.12553.

[63] A. M. Leroi, A. F. Bennett, and R. E. Lenski. Temperature acclimation and competitive fitness: an experimental test of the beneficial acclimation assumption. *Proceedings of the National Academy of Sciences*, 91(5):1917–1921, 1994. doi: 10.1073/pnas.91.5.1917. URL https://www.pnas.org/doi/abs/10.1073/pnas.91.5.1917.

[64] G. Li, Y. Hu, J. Zrimec, H. Luo, H. Wang, A. Zelezniak, B. Ji, and J. Nielsen. Bayesian genome scale modelling identifies thermal determinants of yeast metabolism. *Nature Communications*, 12, 01 2021. doi: 10.1038/s41467-020-20338-2.

[65] L. L. Liang, V. L. Arcus, M. A. Heskel, O. S. O'Sullivan, L. K. Weerasinghe, D. Creek, J. J. Egerton, M. G. Tjoelker, O. K. Atkin, and L. A. Schipper. Macromolecular rate theory (mmrt) provides a thermodynamics rationale to underpin the convergent temperature response in plant leaf respiration. *Global Change Biology*, 24(4):1538–1547, 2018.

[66] L. Liu and Q.-X. Guo. Isokinetic relationship, isoequilibrium relationship, and enthalpyentropy compensation. *Chemical Reviews*, 101(3):673–696, 2001. doi: 10.1021/cr990416z. URL https://doi.org/10.1021/cr990416z. PMID: 11712500.

[67] T. Lonhienne, C. Gerday, and G. Feller. Psychrophilic enzymes: revisiting the thermodynamic parameters of activation may explain local flexibility. *Biochimica et Biophysica Acta (BBA)-Protein Structure and Molecular Enzymology*, 1543(1):1–10, 2000.

[68] P. S. Low, J. L. Bada, and G. N. Somero. Temperature adaptation of enzymes: Roles of the free energy, the enthalpy, and the entropy of activation. *Proceedings of the National Academy of Sciences*, 70(2):430–432, 1973. doi: 10.1073/pnas.70.2.430. URL https://www.pnas.org/doi/abs/10.1073/pnas.70.2.430.

[69] T. M. Luhring and J. P. DeLong. Scaling from Metabolism to Population Growth Rate to Understand How Acclimation Temperature Alters Thermal Performance. *Integrative and Comparative Biology*, 57(1):103–111, 06 2017. ISSN 1540-7063. doi: 10.1093/icb/icx041. URL https://doi.org/10.1093/icb/icx041.

[70] T. Martin and R. Huey. Why "suboptimal" is optimal: Jensen's inequality and ectotherm thermal preferences. *The American Naturalist*, 171(3):E102–E118, 2008. doi: 10.1086/527502. URL https://doi.org/10.1086/527502. PMID: 18271721.

[71] M. W. McCoy and J. F. Gillooly. Predicting natural mortality rates of plants and animals. *Ecology letters*, 11(7):710–716, 2008.

[72] M. A. Mowery, S. E. Anthony, A. N. Dorison, A. C. Mason, and M. C. B. Andrade. Invasive Widow Spiders Perform Differently at Low Temperatures from Conspecifics from the Native Range. *Integrative and Comparative Biology*, 62(2):179–190, 06 2022. ISSN 1540-7063. doi: 10.1093/icb/icac073. URL https://doi.org/10.1093/icb/icac073.

[73] V. Nguyen, C. Wilson, M. Hoemberger, J. B. Stiller, R. V. Agafonov, S. Kutter, J. English, D. L. Theobald, and D. Kern. Evolutionary drivers of thermoadaptation in enzyme catalysis. *Science*, 355(6322):289–294, 2017. doi: 10.1126/science.aah3717. URL https://www.science.org/doi/abs/10.1126/science.aah3717.

[74] J. Norberg, M. Urban, M. Vellend, C. Klausmeier, and N. Loeuille. Eco-evolutionary responses of biodiversity to climate change. *Nat. Clim. Change*, 2:747–751, 07 2012. doi: 10.1038/nclimate1588.

[75] R. G. Pearson and T. P. Dawson. Predicting the impacts of climate change on the distribution of species: are bioclimate envelope models useful? *Global Ecology and Biogeography*, 12(5):361–371, 2003. ISSN 1466-8238. doi: 10.1046/j.1466-822X.2003.00042.x. URL https://onlinelibrary.wiley.com/doi/abs/10.1046/j.1466-822X.2003.00042.x.

[76] M. M. Pinney, D. A. Mokhtari, E. Akiva, F. Yabukarski, D. M. Sanchez, R. Liang, T. Doukov, T. J. Martinez, P. C. Babbitt, and D. Herschlag. Parallel molecular mechanisms for enzyme temperature adaptation. *Science*, 371(6533):eaay2784, 2021. doi: 10.1126/science.aay2784. URL https://www.science.org/doi/abs/10.1126/science.aay2784.

[77] H. Pörtner, A. Bennett, F. Bozinovic, A. Clarke, M. Lardies, M. Lucassen, B. Pelster, F. Schiemer, and J. Stillman. Trade-offs in thermal adaptation: The need for a molecular to ecological integration. *Physiological and Biochemical Zoology*, 79(2):295–313, 2006. doi: 10.1086/499986. URL https://doi.org/10.1086/499986. PMID: 16555189.

[78] T. D. Price, A. Qvarnström, and D. E. Irwin. The role of phenotypic plasticity in driving genetic evolution. *Proceedings of the Royal Society of London. Series B: Biological Sciences*, 270(1523):1433–1440, 2003. doi: 10.1098/rspb.2003.2372. URL https://royalsocietypublishing.org/doi/abs/10.1098/rspb.2003.2372.

[79] Z. Qin, S. K. Balasubramanian, W. F. Wolkers, J. A. Pearce, and J. C. Bischof. Correlated Parameter Fit of Arrhenius Model for Thermal Denaturation of Proteins and Cells. *Annals of Biomedical Engineering*, 42(12):2392–2404, Dec. 2014. ISSN 1573-9686. doi: 10.1007/s10439-014-1100-y. URL https://doi.org/10.1007/s10439-014-1100-y.

[80] N. Rank and E. Dahlhoff. Allele frequency shifts in response to climate change and physiological consequences of allozyme variation in a montane insect. *Evolution; international journal of organic evolution*, 56:2278–89, 11 2002. doi: 10.1554/0014-3820(2002)056[2278:AFSIRT]2.0.CO;2.

[81] D. A. Ratkowsky, J. Olley, and T. Ross. Unifying temperature effects on the growth rate of bacteria and the stability of globular proteins. *J. Theor. Biol.*, 233(3):351–362, 2005. ISSN 0022-5193. doi: https://doi.org/10.1016/j.jtbi.2004.10.016. URL https://www.sciencedirect.com/science/article/pii/S0022519304004941.

[82] D. A. Ratkowsky, J. Olley, and T. Ross. Unifying temperature effects on the growth rate of bacteria and the stability of globular proteins. *Journal of Theoretical Biology*, 233(3):351–362, 2005. ISSN 0022-5193. doi: https://doi.org/10.1016/j.jtbi.2004.10.016. URL https://www.sciencedirect.com/science/article/pii/S0022519304004941.

[83] A. Razvi and J. M. Scholtz. Lessons in stability from thermophilic proteins. *Protein Science*, 15(7):1569–1578, 2006.

[84] B. Rosenberg, G. Kemeny, R. C. Switzer, and T. C. Hamilton. Quantitative Evidence for Protein Denaturation as the Cause of Thermal Death. *Nature*, 232(5311):471–473, Aug. 1971. ISSN 1476-4687. doi: 10.1038/232471a0. URL https://www.nature.com/articles/232471a0.

[85] P. C. l. Roux, L. Pellissier, M. S. Wisz, and M. Luoto. Incorporating dominant species as proxies for biotic interactions strengthens plant community models. *Journal of Ecology*, 102(3):767–775, May 2014. ISSN 1365-2745. URL https://onlinelibrary.wiley.com/doi/abs/10.1111/1365-2745.12239.

[86] M. Saastamoinen. Heritability of dispersal rate and other life history traits in the glanville fritillary butterfly. *Edinb*, 100:39–46, 2008.

[87] M. Saastamoinen, I. Hanski, A. E. G. W. Gilchrist, and E. M. C. Whitlock. Genotypic and environmental effects on flight activity and oviposition in the glanville fritillary butterfly. *The American Naturalist*, 171(6):701–712, 2008. ISSN 00030147, 15375323. URL http://www.jstor.org/stable/10.1086/587531.

[88] H. Saavedra, J. Wrabl, J. Anderson, J. Li, and V. Hilser. Dynamic allostery can drive cold adaptation in enzymes. *Nature*, 558, 06 2018. doi: 10.1038/s41586-018-0183-2.

[89] S. M. Scheiner, M. Barfield, and R. D. Holt. The genetics of phenotypic plasticity. xv. genetic assimilation, the baldwin effect, and evolutionary rescue. *Ecology and Evolution*, 7(21):8788–8803, 2017. doi: https://doi.org/10.1002/ece3.3429. URL https://onlinelibrary.wiley.com/doi/abs/10.1002/ece3.3429.

[90] R. Schoolfield, P. Sharpe, and C. Magnuson. Non-linear regression of biological temperature-dependent rate models based on absolute reaction-rate theory. *Journal of Theoretical Biology*, 88(4):719–731, 1981. ISSN 0022-5193. doi: https:

//doi.org/10.1016/0022-5193(81)90246-0. URL https://www.sciencedirect.com/science/article/pii/0022519381902460.

[91] P. M. Schulte, T. M. Healy, and N. A. Fangue. Thermal Performance Curves, Phenotypic Plasticity, and the Time Scales of Temperature Exposure. *Integrative and Comparative Biology*, 51(5):691–702, 08 2011. ISSN 1540-7063. doi: 10.1093/icb/icr097. URL https://doi.org/10.1093/icb/icr097.

[92] P. M. Schulte, J. E. Podrabsky, J. H. Stillman, and L. Tomanek. The effects of temperature on aerobic metabolism: towards a mechanistic understanding of the responses of ectotherms to a changing environment. *Journal of Experimental Biology*, 218(12):1856–1866, 06 2015. ISSN 0022-0949. doi: 10.1242/jeb.118851. URL https://doi.org/10.1242/jeb.118851.

[93] A. Sentis, J.-L. Hemptinne, and J. Brodeur. Using functional response modeling to investigate the effect of temperature on predator feeding rate and energetic efficiency. *Oecologia*, 169(4):1117—1125, August 2012. ISSN 0029-8549. doi: 10.1007/s00442-012-2255-6. URL https://doi.org/10.1007/s00442-012-2255-6.

[94] K. S. Siddiqui. Defying the activity–stability trade-off in enzymes: taking advantage of entropy to enhance activity and thermostability. *Critical Reviews in Biotechnology*, 37(3):309–322, 2017. doi: 10.3109/07388551.2016.1144045. URL https://doi.org/10.3109/07388551.2016.1144045. PMID: 26940154.

[95] B. J. Sinclair, C. M. Williams, and J. S. Terblanche. Variation in thermal performance among insect populations. *Physiological and biochemical zoology*, 85(6):594–606, 2012.

[96] G. N. Somero. Proteins and temperature. *Annual Review of Physiology*, 57(1):43–68, 1995. doi: 10.1146/annurev.ph.57.030195.000355. URL https://doi.org/10.1146/annurev.ph.57.030195.000355. PMID: 7778874.

[97] Stan Development Team. RStan: the R interface to Stan, 2022. URL https://mc-stan.org/. R package version 2.21.7.

[98] C. Stark, T. Bautista-Leung, J. Siegfried, and D. Herschlag. Systematic investigation of the link between enzyme catalysis and cold adaptation. *eLife*, 11:e72884, jan 2022. ISSN 2050-084X. doi: 10.7554/eLife.72884. URL https://doi.org/10.7554/eLife.72884.

[99] T. N. Starr and J. W. Thornton. Epistasis in protein evolution. *Protein Science*, 25(7):1204–1218, 2016. doi: https://doi.org/10.1002/pro.2897. URL https://onlinelibrary.wiley.com/doi/abs/10.1002/pro.2897.

[100] S. E. Sultan and H. G. Spencer. Metapopulation structure favors plasticity over local adaptation.. *The American Naturalist*, 160(2):271–283, 2002. doi: 10.1086/341015. URL https://doi.org/10.1086/341015. PMID: 18707492.

[101] H. R. Thieme. *Mathematics in Population Biology*. PUP, Princeton, NY, USA, 2003.

[102] W. Uszko, S. Diehl, G. Englund, and P. Amarasekare. Effects of warming on predator–prey interactions – a resource-based approach and a theoretical synthesis. *Ecology Letters*, 20(4):513–523, 2017. doi: https://doi.org/10.1111/ele.12755. URL https://onlinelibrary.wiley.com/doi/abs/10.1111/ele.12755.

[103] D. A. Vasseur, J. P. DeLong, B. Gilbert, H. S. Greig, C. D. G. Harley, K. S. McCann, V. Savage, T. D. Tunney, and M. I. O'Connor. Increased temperature variation poses a greater risk to species than climate warming. *Proceedings of the Royal Society B: Biological Sciences*, 281(1779):20132612, 2014. doi: 10.1098/rspb.2013.2612. URL https://royalsocietypublishing.org/doi/abs/10.1098/rspb.2013.2612.

[104] A. Vehtari, A. Gelman, and J. Gabry. Practical bayesian model evaluation using leave-one-out cross-validation and waic. *Statistics and computing*, 27(5):1413–1432, 2017.

[105] C. Vieille and G. J. Zeikus. Hyperthermophilic enzymes: Sources, uses, and molecular mechanisms for thermostability. *Microbiology and Molecular Biology Reviews*, 65(1): 1–43, 2001. doi: 10.1128/MMBR.65.1.1-43.2001. URL https://journals.asm.org/doi/abs/10.1128/MMBR.65.1.1-43.2001.

[106] S. Watanabe and M. Opper. Asymptotic equivalence of bayes cross validation and widely applicable information criterion in singular learning theory. *Journal of machine learning research*, 11(12), 2010.

[107] D. M. Weinreich, N. F. Delaney, M. A. DePristo, and D. L. Hartl. Darwinian evolution can follow only very few mutational paths to fitter proteins. *Science*, 312(5770):111–114, 2006. doi: 10.1126/science.1123539. URL https://www.science.org/doi/abs/10.1126/science.1123539.

[108] E. E. Werner and B. R. Anholt. Ecological consequences of the trade-off between growth and mortality rates mediated by foraging activity. *The American Naturalist*, 142(2):242–272, 1993.

[109] C. R. White, L. A. Alton, and P. B. Frappell. Metabolic cold adaptation in fishes occurs at the level of whole animal, mitochondria and enzyme. *Proceedings of the Royal Society B: Biological Sciences*, 279(1734):1740–1747, 2012. doi: 10.1098/rspb.2011.2060. URL https://royalsocietypublishing.org/doi/abs/10.1098/rspb.2011.2060.

[110] R. J. Woods, J. E. Barrick, T. F. Cooper, U. Shrestha, M. R. Kauth, and R. E. Lenski. Second-order selection for evolvability in a large ¡i¿escherichia coli¡/i¿ population. *Science*, 331(6023):1433–1436, 2011. doi: 10.1126/science.1198914. URL https://www.science.org/doi/abs/10.1126/science.1198914.

[111] J. Y. Xia, R. Rabbinge, and W. Van Der Werf. Multistage Functional Responses in a Ladybeetle-Aphid System: Scaling up from the Laboratory to the Field. *Environmental Entomology*, 32(1):151–162, 02 2003. ISSN 0046-225X. doi: 10.1603/0046-225X-32.1.151. URL https://doi.org/10.1603/0046-225X-32.1.151.

[112] Y. Yao, A. Vehtari, D. Simpson, and A. Gelman. Using stacking to average bayesian predictive distributions (with discussion). *Bayesian Analysis*, 13(3):917–1007, 2018.

[113] K. B. Zeldovich, P. Chen, and E. I. Shakhnovich. Protein stability imposes limits on organism complexity and speed of molecular evolution. *Proceedings of the National Academy of Sciences*, 104(41):16152–16157, 2007. doi: 10.1073/pnas.0705366104. URL https://www.pnas.org/doi/abs/10.1073/pnas.0705366104.

[114] P. Závodszky, J. Kardos, Ádám Svingor, and G. A. Petsko. Adjustment of conformational flexibility is a key event in the thermal adaptation of proteins. *Proceedings of the National Academy of Sciences*, 95(13):7406–7411, 1998. doi: 10.1073/pnas.95.13.7406. URL https://www.pnas.org/doi/abs/10.1073/pnas.95.13.7406.